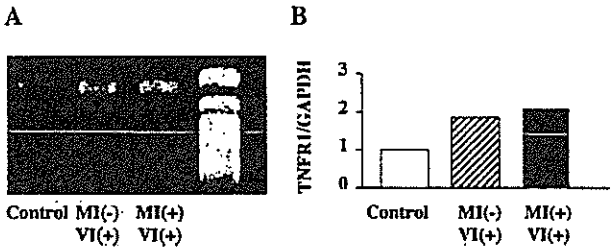

Figure 4. Effect of vascular injury on arterial expression of TNFR1. Tissue samples were prepared from injured and uninjured (control) femoral arteries 14 days after surgery: A, A representative image of RT-PCRs for TNFR1 expression. B, Quantitative real-time PCR analysis of TNFR1 expression levels obtained from 3 to 4 mice in each group.

Discussion

The main findings of the present study are that: (1) the inflammatory response to AMI augments neointimal hyperplasia at sites of injury within distant arteries; (2) BM-derived cells contribute to neointimal hyperplasia after vascular injury, but not to the AMI-related augmentation of the response; (3) cardiac synthesis of TNF-α and circulating TNF-α levels are both increased after AMI, as is expression of TNFR1 mRNA in injured arteries; (4) IL-6 is preferentially upregulated in the neointima of injured arteries after AMI; and (5) treatment with PTX, an inhibitor of TNF-α synthesis, inhibited the AMI-induced increases in plasma TNF-α and attenuated neointima formation after vascular injury. It thus appears that the inflammatory response to AMI stimulates neointimal hyperplasia at sites of vascular injury at least in part by stimulating signaling via TNF-α, TNFR1, and IL-6.

Cardiac levels of several vasoactive cytokines are elevated after AMI. For instance, levels of VEGF are increased in both infarcted hearts and the plasma. We also have observed that plasma levels of placental growth factor (PlGF), another VEGF family cytokine, are elevated within infarcted hearts as a result of its synthesis in endothelial cells within the infarcted region.[23] Earlier works by Hattori et al indicate that both VEGF and PlGF stimulate matrix metalloproteinase (MMP)-9 expression in BM stromal cells via the flt pathway, and that MMP-9 cleaves membrane bound Kit ligand into soluble Kit ligand, which in turn activates hematopoietic stem cells.[24,25] In addition, numbers of CD34-positive cells also are increased after AMI.[13] Based on these findings, we suggested that conditions directly caused by AMI stimulate neointimal hyperplasia at remote sites of vascular injury, and that BM-derived cells contribute significantly to the AMI-related augmentation of neointimal hyperplasia. In that regard, one recent report showed that BM-derived cells contribute to neointimal hyperplasia after mechanical vascular injury, especially after severe wire-induced injury.[26] In the present

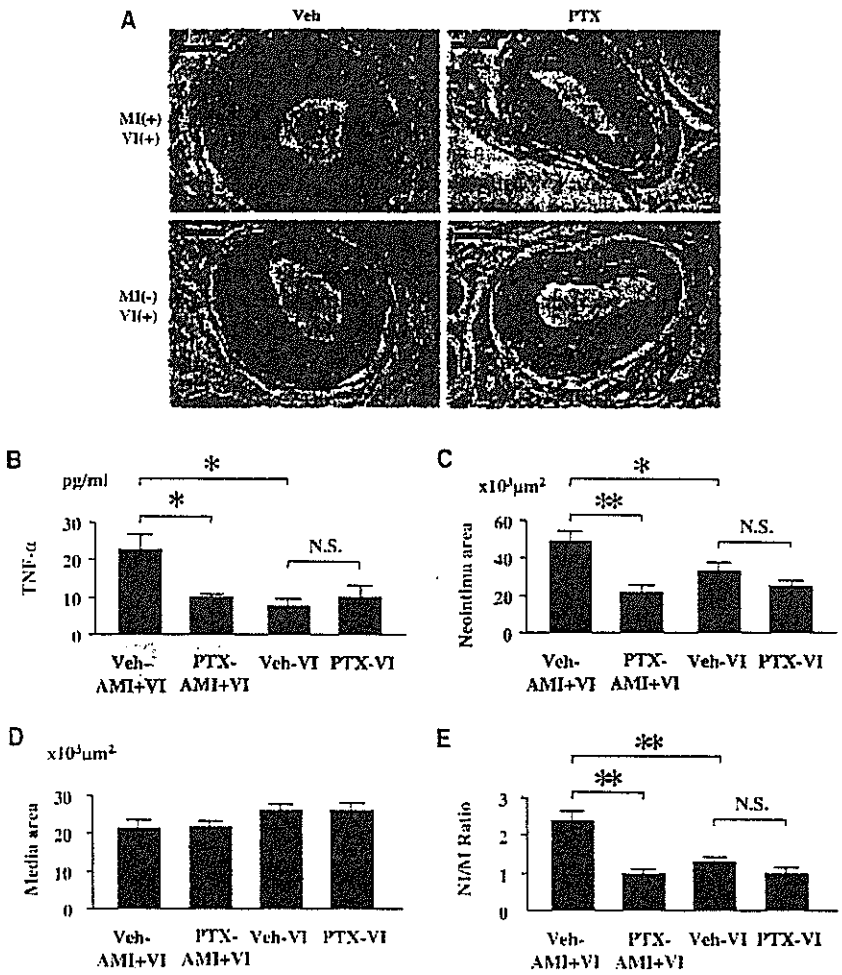

Figure 5. Inhibitory effect of PTX in AMI+VI and VI mice. A, Hematoxylin and eosin-stained sections of femoral artery from Veh-treated AMI+VI, Veh-treated VI, PTX-treated AMI+VI, and PTX-treated VI mice (8 to 10 weeks old) harvested 4 weeks after vascular injury; scale bars represent 100 μm. B, Circulating TNF-α levels in AMI+VI and VI mice continuously infused for 4 weeks with Veh or PTX. C to E, Effect of PTX treatment on morphological changes. Morphometric analysis of injured femoral arteries in AMI+VI and VI mice, with or without PTX, 4 weeks after wire-induced injury. Values are mean±SEM; *$P<0.05$; **$P<0.01$; n=6 to 10; N.S indicates not statistically significant.

study, we confirmed the presence of BM-derived cells in the neointima and media of the affected artery after wire-induced vascular injury. But as shown in Figure 2, although the number of neointimal BM-derived cells tended to be higher in mice after AMI than after sham operation, the difference was not sufficient to explain the augmented neointimal hyperplasia seen after AMI. Apparently, AMI does not stimulate recruitment of BM-derived cells into the neointima at sites of vascular injury. Pathological significance of BM-derived cells in the setting of AMI is needed to be further elucidated.

Our analysis of cDNA arrays, performed to identify key molecules responsible for the AMI-related augmentation of neointimal hyperplasia after vascular injury, revealed upregulation of MCP-1, VEGF, TGF-β, SDF-1α, and IL-1β within injured arteries, with and without AMI. However, levels of IL-6 were $\approx$7-fold higher in the injured arteries of AMI+VI mice than in those of VI mice. Studies have shown that IL-6 mRNA is expressed in the atherosclerotic lesions of apolipoprotein E knockout mice[27] and humans[28,29] and in the neointimas of injured arteries,[5] and that STAT3, which is activated by IL-6, contributes to neointima formation by promoting neointimal SMC proliferation and survival.[30] However, earlier reports mainly emphasized the importance of MCP-1, VEGF, TGF-β,SDF-1α, and IL-1β rather than IL-6 in neointima formation. The present study confirms the importance of IL-6 in neointimal hyperplasia after wire-induced injury and suggests that IL-6 plays a more important role in AMI-related neointimal hyperplasia than the other aforementioned mediators.

Bearing that in mind, a key question is, what are the signals that stimulate the preferential elevation of IL-6 expression in injured arteries after AMI? A number of earlier reports have shown that TNF-α and IL-1β are strong stimulators of IL-6 expression.[22,31] Consistent with that earlier work, we found that TNF-α expression is upregulated in infarcted hearts during the 2-week period after AMI and that plasma TNF-α levels were increased to 22.6$\pm$4.2 pg/mL, which is sufficient to stimulate IL-6 expression.[32–34] We also detected expression of TNFR1 mRNA in injured arteries, but not in healthy ones. TNF-α exerts its effects through both TNFR1 and TNFR2, but blockade of TNFR1 gene expression reportedly reduces neointimal hyperplasia after vascular injury by 2-fold, whereas blocking TNFR2 expression has no effect.[35] Thus, in the setting of AMI, it is likely that TNF-α released from the infarcted heart binds to newly upregulated-TNFR1 on the surface of cells at remote sites of arterial injury, leading to IL-6 production and, ultimately, stimulation of neointimal hyperplasia.

To prove a cause–effect relationship between expression of TNF-α in heart and IL-6 in arteries, and one between AMI and augmented neointima formation, we demonstrated that prevention of TNF-α synthesis by PTX inhibited the AMI-induced increases in plasma TNF-α and attenuated neointimal formation after vascular injury. Collectively, these results are indicative of the important role played by TNF-α in experimental postangioplasty restenosis. An earlier report showed the short-term, exogenous administration of TNF-α did not increase neointima formation after balloon injury in rabbits,[36] suggesting that prolonged and persistent elevation of circulating TNF-α is required to promote neointimal hyperplasia after vascular injury. In this study, we used PTX as an inhibitor of TNF-α synthesis instead of a neutralizing antibody or a soluble form of TNF-α receptor. Although both neutralizing antibody and soluble form of TNF-αreceptor are more specific than PTX, they are immunogenic,[37] when they are used in vivo experiments especially in the long-term experiment like the present experiment. PTX reduces the synthesis of TNF-α by blocking its transcription,[38] and has been used successfully in earlier works.[39,40] Therefore, we adopted PTX to inhibit TNF-α pathway. However, it might be possible that present findings were modulated by other molecules transcriptionally suppressed by PTX.

In the clinical point of view, primary purpose of the present study is to elucidate whether post-AMI conditions enhance the neointimal hyperplasia and restenosis after PCI, that is why we generated a mouse model of AMI plus vascular injury. However, further studies using model in larger animal such as porcine are necessary to get more directly evidence that AMI augments neointimal hyperplasia and restenosis after PCI of infarct-related artery.

In conclusion, the present findings provide experimental evidence supporting the idea that conditions directly resulting from AMI exacerbate neointimal hyperplasia after vascular injury through activation of TNF-α, TNFR1, and IL-6 network.

Acknowledgments

We thank Professor M. Okabe, Osaka University, Osaka, Japan, for providing us with GFP Tg mice.

Sources of Funding

This work was supported in part by research grants from the Japanese Ministry of Health, Labor and Welfare, the Japanese Society for the Promotion of Science, and the Japan Health Science Foundation, and a Japan Heart Foundation/Pfizer Japan Grant on Cardiovascular Disease Research.

Disclosures

None.

References

1. Hansson GK. Immune mechanisms in atherosclerosis. *Arterioscler Thromb Vasc Biol.* 2001;21:1876–1890.
2. Angioi M, Abdelmouttaleb I, Rodriguez RM, Aimone-Gastin I, Adjalla C, Guéant JL, Danchin N. Increased C-reactive protein levels in patients with in-stent restenosis and its implications. *Am J Cardiol.* 2001;87:1189–1193.
3. Farb A, Sangiorgi G, Carter AJ, Walley VM, Edwards WD, Schwartz RS, Virmani R. Pathology of acute and chronic coronary stenting in humans. *Circulation.* 1999;99:44–52.
4. Serrano CV Jr., Ramires JA, Venturinelli M, Aric S, D'Amico E, Zweier JL, Pileggi F, da Luz PL. Coronary angioplasty results in leukocyte and platelet activation with adhesion molecule expression. Evidence of inflammatory responses in coronary angioplasty. *J Am Coll Cardiol.* 1997;29:1276–1283.
5. Wu L, Iwai M, Nakagami H, Li Z, Chen R, Suzuki J, Akishita M, Gasparo MD, Horiuchi M. Roles of angiotensin II type 2 receptor stimulation associated with selective angiotensin II type 1 receptor blockade with Valsartan in the improvement of inflammation-induced vascular injury. *Circulation.* 2001;104:2716–2721.
6. Frangogiannis NG, Smith CW, Entman ML. The inflammatory response in myocardial infarction. *Cardiovasc Res.* 2002;53:31–47.
7. Irwin MW, Mak S, Mann DL, Qu R, Penninger JM, Yan A, Dawood F, Wen WH, Shou Z, Liu P. Tissue expression and immunolocalization of

tumor necrosis factor-α in postinfarction dysfunctional myocardium. *Circulation.* 1999;99:1492–1498.
8. Kukielka GL, Smith CW, Manning AM, Youker KA, Michael LH, Entman ML. Induction of interleukin-6 synthesis in the myocardium. Potential role in post-reperfusion inflammatory injury. *Circulation.* 1995; 92:1866–1875.
9. Lee SH, Wolf PL, Escudero R, Deutsch R, Jamieson SW, Thistlethwaite PA. Early expression of angiogenesis factors in acute myocardial ischemia and infarction. *N Engl J Med.* 2000;342:626–633.
10. Li J, Brown LF, Hibberd MG, Grossman JD, Morgan JP, Simons M. VEGF, flk-1, and flt-1 expression in a rat myocardial infarction model of angiogenesis. *Am J Physiol.* 1996;270:H1803–H1811.
11. Sata M, Saiura A, Kunisato A, Tojo A, Okada S, Tokuhisa T, Hirai H, Makuuchi M, Hirata Y, Nagai R. Hematopoietic stem cells differentiate into vascular cells that participate in the pathogenesis of atherosclerosis. *Nat Med.* 2002;8:403–409.
12. Ross R. Atherosclerosis: an inflammatory disease. *N Engl J Med.* 1999; 340:115–126.
13. Shintani S, Murohara T, Ikeda H, Ueno T, Honma T, Katoh A, Sasaki K, Shimada T, Oike Y, and Imaizumi T. Mobilization of endothelial progenitor cells in patients with acute myocardial infarction. *Circulation.* 2001;103:2776–2779.
14. Massa M, Rosti V, Ferrario M, Campanelli R, Ramajoli I, Rosso R, De Ferrari GM, Ferlini M, Goffredo L, Bertoletti A, Klersy C, Pecci A, Moratti R, Tavazzi L. Increased circulating hematopoietic and endothelial progenitor cells in the early phase of acute myocardial infarction. *Blood.* 2005;105:199–206.
15. Francis J, Chu Y, Johnson AK, Weiss RM, Felder RB. Acute myocardial infarction induces hypothalamic cytokine synthesis. *Am J Physiol Heart Circ Physiol.* 2004;286:H2264–H2271.
16. Waage A, Sorensen M, Stordal B. Differential effect of oxpentifylline on tumour necrosis factor and interleukin-6 production. *Lancet.* 1990; 335:543.
17. Zabel P, Wolter DT, Schonharting MM, Schade UF. Oxpentifylline in endotoxaemia. *Lancet.* 1989;334:1474–1477.
18. Okabe M, Ikawa M, Kominami K, Nakanishi T, Nishimune Y. Green mice as a source of ubiquitous green cells. *FEBS Lett.* 1997;407:313–319.
19. Adachi Y, Saito Y, Kishimoto I, Harada M, Kuwahara K, Takahashi N, Kawakami R, Nakanishi M, Nakagawa Y, Tanimoto K, Saitoh Y, M, Yasuno S, Usami S, Iwai M, Horiuchi M, Nakao K. Angiotensin II type 2 receptor deficiency exacerbates heart failure and reduces survival after acute myocardial infarction in mice. *Circulation.* 2003;107:2406–2408.
20. Izumi T, Saito Y, Kishimoto I, Harada M, Kuwahara K, Hamanaka I, Takahashi N, Kawakami R, Li Y, Takemura G, Fujiwara H, Garbers DL, Mochizuki S, Nakao K. Blockade of the natriuretic peptide receptor guanylyl cyclase-A inhibits NF-κB activation and alleviates myocardial ischemia/reperfusion injury. *J Clin Invest.* 2001;108:203–213.
21. Sata M, Maejima Y, Adachi F, Fukino K, Saiura A, Sugiura S, Aoyagi T, Imai Y, Kurihara H, Kimura K, Omata M, Makuuchi M, Hirata Y, Nagai R. A mouse model of vascular injury that induces rapid onset of medial cell apoptosis followed by reproducible neointimal hyperplasia. *J Mol Cell Cardiol.* 2000;32:2097–2104.
22. Vanden Berghe W, Vermeulen L, De Wilde G, De Bosscher K, Boone E, Haegeman G. Signal transduction by tumor necrosis factor and gene regulation of the inflammatory cytokine interleukin-6. *Biochem Pharmacol.* 2000;60:1185–1195.
23. Iwama H, Uemura S, Naya N, Imagawa K, Takemoto Y, Asai O, Onoue K, Okayama S, Somekawa S, Kida Y, Takeda Y, Takaoka M, Kawata H, Horii M, Nakajima T, Doi N, Saito Y. Cardiac expression of placental growth factor predicts the improvement of chronic phase left ventricular function in patients with acute myocardial infarction. *J Am Coll Cardiol.* 2006;47:1559–1567.
24. Hattori K, Heissig B, Wu Y, Dias S, Tejada R, Ferris B, Hicklin DJ, Zhu Z, Bohlen P, Witte L, Hendrikx J, Hackett NR, Crystal RG, Moore MA, Werb Z, Lyden D, Rafii S. Placental growth factor reconstitutes hematopoiesis by recruiting VEGFR1(+) stem cells from bone-marrow microenvironment. *Nat Med.* 2002;8:841–849.
25. Heissig B, Hattori K, Dias S, Friedrich M, Ferris B, Hackett NR, Crystal RG, Besmer P, Lyden D, Moore MA, Werb Z, Rafii S. Recruitment of stem and progenitor cells from the bone marrow niche requires MMP-9 mediated release of kit-ligand. *Cell.* 2002;109:625–637.
26. Tanaka K, Sata M, Hirata Y, Nagai R. Diverse contribution of bone marrow cells to neointimal hyperplasia after mechanical vascular injuries. *Circ Res.* 2003;93:783–790.
27. Sukovich DA, Kauser K, Shirley FD, DelVecchio V, Halks-Miller M, Rubanyi GM. Expression of interleukin-6 in atherosclerotic lesions of male ApoE-knockout mice: inhibition by 17beta-estradiol. *Arterioscler Thromb Vasc Biol.* 1998;18:1498–1505.
28. Rus HG, Vlaicu R, Niculescu F. Interleukin-6 and interleukin-8 protein and gene expression in human arterial atherosclerotic wall. *Atherosclerosis.* 1996;127:263–271.
29. Seino Y, Ikeda U, Ikeda M, Yamamoto K, Misawa Y, Hasegawa T, Kano S, Shimada K. Interleukin 6 gene transcripts are expressed in human atherosclerotic lesions. *Cytokine.* 1994;6:87–91.
30. Shibata R, Kai H, Seki Y, Kato S, Wada Y, Hanakawa Y, Hashimoto K, Yoshimura A, Imaizumi T. Inhibition of STAT3 prevents neointima formation by inhibiting proliferation and promoting apoptosis of neointimal smooth muscle cells. *Hum Gene Ther.* 2003;14:601–610.
31. Loppnow H, Libby P. Proliferating or interleukin 1-activated human vascular smooth muscle cells secrete copious interleukin 6. *J Clin Invest.* 1990;85:731–738.
32. Francis J, Zhang ZH, Weiss RM, Felder RB. Neural regulation of the proinflammatory cytokine response to acute myocardial infarction. *Am J Physiol Heart Circ Physiol.* 2004;287:H791–H797.
33. Selzman CH, Shames BD, Reznikov LL, Miller SA, Meng X, Barton HA, Werman A, Harken AH, Dinarello CA, Banerjee A. Liposomal delivery of purified inhibitory-κBa inhibits tumor necrosis factor-α–induced human vascular smooth muscle proliferation. *Circ Res.* 1999;84: 867–875.
34. Ridker PM, Rifai N, Pfeffer M, Sacks F, Lepage S, Braunwald E. for the Cholesterol And Recurrent Events (CARE) Investigators. Elevation of tumor necrosis factor-α and increased risk of recurrent coronary events after myocardial infarction. *Circulation.* 2000;101:2149–2153.
35. Zimmerman MA, Reznikov LL, Sorensen AC, Selzman CH. Relative contribution of the TNF-alpha receptors to murine intimal hyperplasia. *Am J Physiol Regul Integr Comp Physiol.* 2003;284:R1213–1218.
36. Miller AM, McPhaden AR, Preston A, Wadsworth RM, Wainwright CL. TNFalpha increases the inflammatory response to vascular balloon injury without accelerating neointimal formation. *Atherosclerosis.* 2005;179: 51–59.
37. Douglas L. Mann. Inflammatory mediators and the failing heart. Past, present, and the foreseeable future. *Circ Res.* 2002;91:988–998.
38. Strieter RM, Remick DG, Ward PA, Spengler RN, Lynch JP 3rd, Larrick J, Kunkel SL. Cellular and molecular regulation of tumor necrosis factor-alpha production by pentoxifylline. *Biochem Biophys Res Commun.* 1988;155:1230–1236.
39. Sliwa K, Skudicky D, Candy G, Wisenbaugh T, Sareli P. Randomised investigation of effects of pentoxifylline on left ventricular performance in idiopathic dilated cardiomyopathy. *Lancet.* 1998;351:1091–1093.
40. Sliwa K, Woodiwiss A, Kone VN, Candy G, Badenhorst D, Norton G, Zambakides C, Peters F, Essop R. Therapy of ischemic cardiomyopathy with the immunomodulating agent pentoxifylline: results of a randomized study. *Circulation.* 2004;109:750–755.

Available online at www.sciencedirect.com

SCIENCE DIRECT

Metabolism Clinical and Experimental 55 (2006) 300–308

Metabolism
Clinical and Experimental

www.elsevier.com/locate/metabol

α2 Isoform–specific activation of 5′ adenosine monophosphate–activated protein kinase by 5-aminoimidazole-4-carboxamide-1-β-D-ribonucleoside at a physiological level activates glucose transport and increases glucose transporter 4 in mouse skeletal muscle

Masako Nakano[a], Taku Hamada[a], Tatsuya Hayashi[a,b,*], Shin Yonemitsu[a], Licht Miyamoto[a], Taro Toyoda[c], Satsuki Tanaka[a], Hiroaki Masuzaki[a], Ken Ebihara[a], Yoshihiro Ogawa[a], Kiminori Hosoda[a], Gen Inoue[a], Yasunao Yoshimasa[a], Akira Otaka[d], Toru Fushiki[c], Kazuwa Nakao[a]

[a]*Department of Medicine and Clinical Science, Kyoto University Graduate School of Medicine, Kyoto 606-8507, Japan*
[b]*Kyoto University Graduate School of Human and Environmental Studies, Kyoto 606-8501, Japan*
[c]*Division of Food Science and Biotechnology, Kyoto University Graduate School of Agriculture, Kyoto 606-8502, Japan*
[d]*Department of Bioorganic Medicinal Chemistry, Kyoto University Graduate School of Pharmaceutical Sciences, Kyoto 606-8501, Japan*

Received 27 October 2004; accepted 24 September 2005

Abstract

5′ Adenosine monophosphate–activated protein kinase (AMPK) has been implicated in exercise-induced stimulation of glucose metabolism in skeletal muscle. Although skeletal muscle expresses both the α1 and α2 isoforms of AMPK, the α2 isoform is activated predominantly in response to moderate-intensity endurance exercise in human and animal muscles. The purpose of this study was to determine whether activation of α2 AMPK plays a role in increasing the rate of glucose transport, promoting glucose transporter 4 (GLUT4) expression, and enhancing insulin sensitivity in skeletal muscle. To selectively activate the α2 isoform, we used 5-aminoimidazole-4-carboxamide-1-β-D-ribonucleoside (AICAR), which is metabolized in muscle cells and preferentially stimulates the α2 isoform. Subcutaneous administration of 250 mg/kg AICAR activated the α2 isoform for 90 minutes, but not the α1 isoform in hind limb muscles of the C57/B6J mouse. The maximal activation of the α2 isoform was observed 30 to 60 minutes after administration of AICAR and was similar to the activation induced by a 30-minute swim in a current pool. The increase in α2 activity paralleled the phosphorylation of Thr^{172}, the essential residue for full kinase activation, and the activity of acetyl-coenzyme A carboxylase β, a known substrate of AMPK in skeletal muscle. Subcutaneous injection of AICAR rapidly increased, by 30%, the rate of 2-deoxyglucose (2DG) transport into soleus muscle; 2DG transport increased within 30 minutes and remained elevated for 4 hours after administration of AICAR. Repeated intraperitoneal injection of AICAR, 3 times a day for 4 to 7 days, increased soleus GLUT4 protein by 30% concomitant with a significant 20% increase in insulin-stimulated 2DG transport. These data suggest that moderate endurance exercise promotes glucose transport, GLUT4 expression, and insulin sensitivity in skeletal muscle at least partially via activation of the α2 isoform of AMPK.

1. Introduction

Physical exercise is a potent stimulator of glucose transport and glucose transporter 4 (GLUT4) expression in skeletal muscle. An acute bout of exercise increases the rate of glucose transport into contracting muscles by inducing translocation of GLUT4 to the cell surface via an insulin-independent mechanism (contraction-stimulated glucose transport) [1]. Acute exercise also activates expression of GLUT4 protein, and the GLUT4 protein expression is elevated with repeated bouts of acute exercise [2]. The exercise-induced increase in GLUT4 is associated with improved insulin sensitivity (ie, increased rates of insulin-stimulated GLUT4 translocation and glucose transport into

* Corresponding author. Kyoto University Graduate School of Human and Environmental Studies, Kyoto 606-8501, Japan. Tel.: +81 75 753 6640; fax: +81 75 753 6640.
E-mail address: tatsuya@kuhp.kyoto-u.ac.jp (T. Hayashi).

0026-0495/$ – see front matter © 2006 Elsevier Inc. All rights reserved.
doi:10.1016/j.metabol.2005.09.003

skeletal muscle) [3]. These mechanisms of enhanced glucose transport help improve glycemic control in patients with diabetes and may help prevent nondiabetic subjects from developing glucose intolerance.

Recent studies have suggested that 5′ adenosine monophosphate–activated protein kinase (AMPK) is an important signaling intermediary leading to contraction-stimulated GLUT4 translocation and glucose transport [4-9] and GLUT4 expression [10-15] in skeletal muscle. AMPK is a heterotrimeric protein composed of a catalytic α subunit and regulatory subunits, β and γ. Although the α subunit exists in different isoforms in skeletal muscle [16], α1 and α2, the α2 isoform–containing AMPK is preferentially activated in response to exercise. For example, cycle ergometer exercise at 50% of maximum energy consumption ($\dot{V}O_2$max) does not change α2 or α1 activity, and exercise at 60% to 75% of $\dot{V}O_2$max increases α2, but not α1, activity in biopsy samples of vastus lateralis muscle from healthy subjects [17-19]. Similar activation of α2 occurs in response to cycle ergometer exercise at 70% of $\dot{V}O_2$max in patients with type 2 diabetes mellitus who have similar protein expression of α isoforms as healthy subjects [20]. In contrast, both isoforms are significantly activated in response to high-intensity exercise such as sprint exercise requiring power output 2- to 3-fold greater than that attained during maximal aerobic exercise [21]. In rat skeletal muscle, voluntary treadmill running exercise increases only α2 activity, whereas high-intensity contractions, such as electrically induced tetanic contractions, increase the activities of both isoforms in isolated rat skeletal muscle [8]. These observations in human and animal muscles suggest that regulation of the α isoforms is intensity-dependent in contracting skeletal muscle, and that the α2 isoform, rather than α1, is involved in the metabolic responses to moderate-intensity endurance exercise.

We explored the physiological relevance of the predominant α2 activation in skeletal muscle, focusing particularly on glucose transport, GLUT4 expression, and insulin sensitivity by selectively activating α2 AMPK using the AMPK-stimulating agent, 5-aminoimidazole-4-carboxamide-1-β-D-ribonucleoside (AICAR).

2. Materials and methods

2.1. Materials

AICAR was obtained from Sigma (St Louis, MO). Phosphospecific antibody directed against AMPKα Thr^{172} was obtained from Cell Signaling Technology (Beverly, MA) and that directed against acetyl-coenzyme A carboxylase β (ACCβ) Ser^{79} from Upstate Biotechnology (Lake Placid, NY). Anti-GLUT4 antibody was obtained from Santa Cruz Biotechnology (Santa Cruz, CA). All radioactive materials were purchased from NEN Life Science Products (Boston, MA). Reagents for the protein assay were obtained from Bio-Rad Laboratories (Hercules, CA). All other chemicals were purchased from Sigma or Nacalai Tesque (Kyoto, Japan) unless otherwise noted.

2.2. Animals

Male C57/B6 mice, aged 7 to 10 weeks, were obtained from Shimizu Breeding Laboratories (Kyoto, Japan) and fed standard laboratory chow and water ad libitum. They were housed in plastic cages in an environmentally controlled room maintained at 23°C with a 12-hour light-dark cycle. Mice were fasted for 8 to 10 hours before the experiments, except as otherwise described. Blood samples were collected from the tail vein. All protocols for animal use and euthanasia were reviewed and approved by the Institute of Laboratory Animals, Graduate School of Medicine, Kyoto University, Japan.

2.3. Administration of AICAR

For studies of a single administration of AICAR, AICAR was dissolved in saline (20 g/L) and injected subcutaneously or intraperitoneally without anesthesia at a dose of 250 mg/kg body weight. Mice were then killed by cervical dislocation at the indicated time points, and either hind limb muscles (gastrocnemius, soleus, tibialis anterior, and extensor digitorum longus [EDL] muscles) or soleus and EDL muscles were dissected. For studies of repeated injections of AICAR, 250 mg/kg of AICAR was dissolved in saline (20 g/L) and injected into fed mice intraperitoneally 3 times a day for up to 8 days. Mice were killed by cervical dislocation 12 to 16 hours after the last injection, and the hind limb or soleus and EDL muscles were collected. The muscles were either processed fresh to measure 2-deoxyglucose (2DG) transport or frozen and stored in liquid nitrogen for later assays. Saline was injected as a control condition in the studies using the single and repeated administration of AICAR.

2.4. Swimming exercise

Mice swam in groups of 6 or less at a time at ~60% of $\dot{V}O_2$max (5 L/min flow rate) for 30 minutes during the dark cycle as described previously [22]. A large adjustable-current pool (90 × 45 × 45 cm) filled to a depth of 38 cm [22] allowed each mouse to swim without interference with other mice. A constant current was generated by circulating water with a pump, and the flow was monitored by a water flow meter, which was used to adjust the strength of the current. The temperature of the water was maintained at 34°C with a water heater and thermostat. For studies involving a single bout of exercise, mice were killed by cervical dislocation immediately after swimming, the hind limb muscles were dissected, and the muscles were frozen and stored in liquid nitrogen. For studies involving repeated bouts of exercise, fed mice swam for 30 minutes during the dark cycle twice a day for up to 7 days. Twelve to 16 hours after the last exercise session, the mice were killed and muscle samples were dissected, frozen, and stored in liquid nitrogen.

2.5. Intraperitoneal glucose test and insulin tolerance test

The intraperitoneal glucose tolerance test (GTT) and insulin tolerance test (ITT) were performed as described [23], with modifications. For the GTT, glucose (2.0 g/kg body weight) was administered intraperitoneally to conscious animals 12 to 16 hours after the last injection of AICAR or saline, or swimming exercise. For the ITT, human recombinant insulin (Eli-Lilly, Indianapolis, IN) (1.2 U/kg body weight diluted with saline) was injected intraperitoneally to fed conscious mice.

2.6. Isoform-specific AMPK activity

Isoform-specific AMPK activity was determined as described [24], with modifications. Frozen muscles were weighed and then homogenized in ice-cold lysis buffer (1:100 wt/vol) containing 20 mmol/L Tris-HCl (pH 7.4), 1% Triton X-100, 50 mmol/L NaCl, 250 mmol/L sucrose, 50 mmol/L NaF, 5 mmol/L sodium pyrophosphate, 2 mmol/L dithiothreitol, 4 mg/L leupeptin, 50 mg/L soybean trypsin inhibitor, 0.1 mmol/L benzamidine, and 0.5 mmol/L phenylmethylsulfonyl fluoride, and centrifuged at 14000*g* for 30 minutes at 4°C. Supernatants (200 μg protein) were immunoprecipitated with specific antibodies against the α1 or α2 catalytic subunit [24] and protein A/G agarose beads (Pierce, Rockford, IL). Immunoprecipitates were washed twice in lysis buffer and twice in wash buffer containing 240 mmol/L HEPES (pH 7.0) and 480 mmol/L NaCl. The kinase reaction, which was started by adding 0.1 mmol/L SAMS peptide with the sequence HMRSAMSGLHLVKRR, contained 40 mmol/L HEPES (pH 7.0), 0.2 mmol/L AMP, 80 mmol/L NaCl, 0.8 mmol/L dithiothreitol, 5 mmol/L $MgCl_2$, and 0.2 mmol/L ATP [2 μCi (γ-^{32}P)ATP] at 30°C for 20 minutes in a final volume of 40 μL. At the end of the reaction, a 15-μL aliquot was removed and spotted onto Whatman P81 paper (Whatman International, Maidstone, UK). The papers were washed 6 times in 1% phosphoric acid and once in acetone. ^{32}P incorporation was quantified with a scintillation counter, and kinase activity was expressed as fold increases relative to basal levels.

2.7. 2-Deoxyglucose transport activity

The amount of 2DG transport was determined as described [25], with modifications. Tendons from both ends of dissected soleus and EDL muscles were tied with sutures (silk 3-0, Natsume Seisakusho, Tokyo, Japan), and the muscles were mounted on an incubation apparatus to maintain resting length. To measure 2DG transport after a single injection of AICAR, muscles were incubated for 10 minutes in 7 mL of incubation buffer containing Krebs-Ringer bicarbonate (KRB) buffer (117 mmol/L NaCl, 4.7 mmol/L KCl, 2.5 mmol/L $CaCl_2$, 2.4 mmol/L KH_2PO_4, 2.4 mmol/L $MgSO_4$, and 24.6 mmol/L $NaHCO_3$) with 2 mmol/L pyruvate and gassed continuously with 95% O_2 and 5% CO_2. Muscles were then transferred to 2 mL of transport buffer containing KRB buffer with 1 mmol/L 2-deoxy-D-[^{3}H]glucose (1.5 mCi/L) and 7 mmol/L D-[^{14}C]mannitol (0.45 mCi/L) at 30°C and incubated for 10 minutes. To measure basal- and insulin-stimulated 2DG transport after repeated AICAR treatment, dissected muscles were preincubated in the incubation buffer for 40 minutes and then incubated in the incubation buffer with or without 5000 mU/L insulin for 40 minutes. Muscles were then transferred to 2 mL of the transport buffer with or without 5000 mU/L insulin and incubated for 10 minutes. Transport was terminated by dipping muscles in KRB at 4°C, and the muscles were frozen in liquid nitrogen. Frozen muscles were weighed and then processed by incubating in 300 μL of 1 mol/L NaOH at 80°C for 10 minutes. Digestates were neutralized with 300 μL of 1 mol/L HCl. Radioactivity in aliquots of the digestates was determined by liquid scintillation counting for dual labels, and the extracellular and intracellular spaces were calculated.

2.8. Muscle glycogen content

Glycogen content was assayed as described [26], with modifications. Frozen muscles were weighed and digested in 1 mol/L NaOH (1:9 wt/vol) at 85°C for 10 minutes. At the end of the incubation, tubes were shaken by hand to facilitate digestion. After cooling to room temperature, digestates were neutralized with 1 mol/L HCl (1:9 wt/vol), and then 5 mol/L HCl was added to obtain a final concentration of 2 mol/L HCl. The digestates were incubated again at 85°C for 2 hours and then neutralized with 5 mol/L NaOH. The concentration of hydrolyzed glucose residues was measured enzymatically using the hexokinase glucose assay reagent (Sigma). Glycogen content was expressed as micromoles of glucose units per gram (wet weight) of muscle.

2.9. Glycogen synthase activity

Glycogen synthase activity was assayed as described [26], with modifications. Frozen muscles were homogenized in buffer containing 20 mmol/L HEPES (pH 7.4), 1% Triton X-100, 50 mmol/L NaCl, 2 mmol/L EGTA, 50 mol/L NaF, 50 mol/L β-glycerophosphate, 10 mg/L aprotinin, 3 mol/L benzamidine, 4 mg/L leupeptin, and 0.5 mol/L phenylmethylsulfonyl fluoride, and centrifuged at 14000*g* for 30 minutes at 4°C. The supernatants (40 μg of protein) were added to 80 μL of reaction solution containing 50 mmol/L Tris-HCl (pH 7.8), 5 mol/L EDTA, 6.7 mmol/L UDP-[^{14}C]glucose (100 μCi/mmol/L), 10 g/L glycogen, 50 mol/L β-glycerophosphate, and 50 mmol/L NaF in the presence or absence of 6.7 mmol/L glucose-6-phosphate at 30°C to measure the glucose-6-phosphate–independent (I-form) and the total glycogen synthase activities, respectively. The reaction was terminated after 15 minutes by spotting the reaction mixture on filter papers; after extensive washing with 66% (vol/vol) ethanol, the samples were counted in a scintillation counter to measure ^{14}C incorporated into glycogen. The enzyme activity was calculated as the ratio of the I-form activity to total activity.

2.10. Immunoblotting

Immunoblotting was performed as described [26], with modifications. Frozen muscles were homogenized in 10 volumes (1:10, wt/vol) of a solution containing 20 mmol/L HEPES (pH 7.4), 50 mmol/L β-glycerophosphate, 2mmol/L EGTA, 1% Triton X-100, 10% glycerol, 1 mmol/L dithiothreitol, 3 mmol/L benzamidine, 1 mmol/L $NaVO_4$, 0.5 mmol/L phenylmethylsulfonyl fluoride, 200 mg/L of soybean trypsin inhibitor, 10 mg/L aprotinin, and 10 mg/L leupeptin. The homogenates were centrifuged at 14000*g* at 4°C for 30 minutes. The supernatants were then diluted with water and Laemmli buffer and boiled at 80°C for 2 minutes. Denatured lysates (20-30 μg protein) were separated on a 10% polyacrylamide gel. Proteins were then transferred to a polyvinylidene difluoride membrane (PolyScreen; Perkin-Elmer, Boston, MA) at 100 V for 1 hour. The membranes were blocked with Block Ace (Yukijirushi Nyugyo, Sapporo, Japan) and left to incubate overnight with antibodies. The membranes were then washed, reacted with antirabbit immunoglobulin G coupled to peroxidase (Santa Cruz Biotechnology), and developed with an enhanced chemiluminescence reagent (Hyperfilm) according to the manufacturer's instructions (Amersham, Uppsala, Sweden). The signal on the blot was detected and quantified with a Lumino-Image Analyzer LAS-1000 System (Fuji Photo Film, Tokyo, Japan). Data were expressed relative to control values.

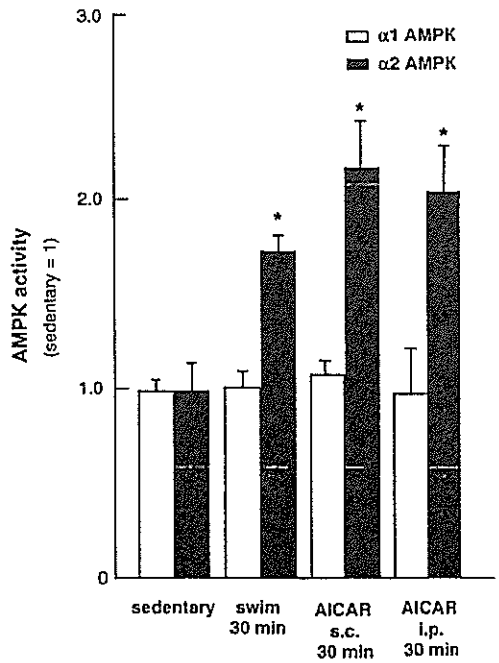

Fig. 1. Effects of exercise and AICAR on α1 and α2 AMPK activities in hind limb muscles. After a 30-minute bout of swimming or 30 minutes after subcutaneous (s.c.) or intraperitoneal (i.p.) injection of 250 mg/kg AICAR, hind limb muscles (gastrocnemius, soleus, tibialis anterior, and EDL) were removed, and isoform-specific AMPK activities were determined. Results are means ± SE (n = 7-10 per group). *P < .05 compared with muscles from sedentary animals.

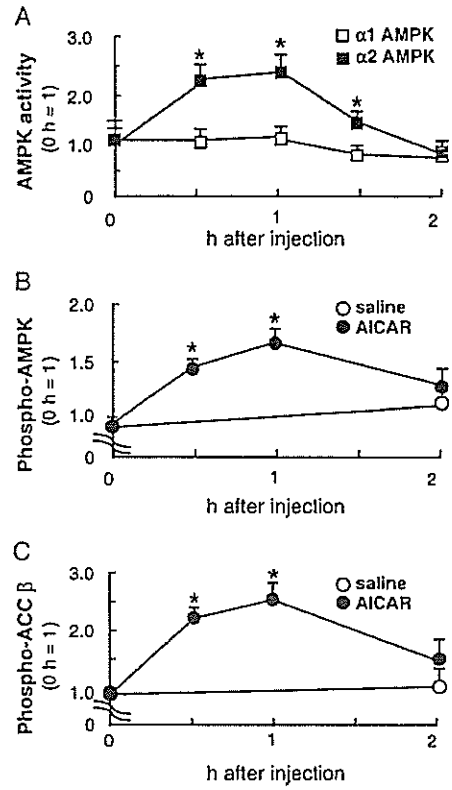

Fig. 2. Time course of changes in isoform-specific AMPK activity (A), AMPK phosphorylation (B), and ACCβ phosphorylation (C) in hind limb muscles after subcutaneous AICAR injection (250 mg/kg). Results are means ± SE (n = 7-10 per group). *P < .05 compared with basal levels.

2.11. Blood lactate, insulin, and glucose concentrations

Blood lactate concentration was measured by the lactate oxidase method using an automated analyzer (Lactate Pro; Arcray, Kyoto, Japan). Serum insulin concentration was determined using an Insulin ELISA kit (Morinaga Institute of Biological Sciences, Yokohama, Japan). Blood glucose concentration was measured by the glucose oxidase method with an automated blood glucose analyzer (Glutest Ace, Sanwa Kagaku, Nagoya, Japan).

2.12. Statistical analysis

Results are presented as means ± SE. Two means were compared by the unpaired Student *t* test. Multiple means were compared by analysis of variance followed by post hoc comparison using the Fisher protected least-significant difference method. P < .05 was considered statistically significant.

3. Results

3.1. Moderate-intensity exercise and AICAR activated predominantly α2 AMPK to a similar extent

After 30 minutes of moderate-intensity swimming exercise, α2 AMPK activity increased by 80%, but α1

AMPK activity did not change significantly in the hind limb muscles (Fig. 1). Similarly, subcutaneous and intraperitoneal injection of AICAR (250 mg/kg) activated α2 AMPK by 110% and 100%, respectively, but did not activate α1 AMPK (Fig. 1). The stimulation of α2 AMPK activity by exercise did not differ significantly from that induced by AICAR injection. The exercise-stimulated activation of α2 was abolished within 2 hours after exercise.

3.2. AICAR increased α2 AMPK activity, AMPK phosphorylation, and ACCβ phosphorylation in skeletal muscle

α2 AMPK activity was significantly higher 30, 60, and 90 minutes after subcutaneous injection of AICAR and returned to baseline within 2 hours after injection in the hind limb muscles (Fig. 2A). α1 AMPK activity did not change at any time point examined (Fig. 2A). Phosphorylation of Thr^{172}, an essential residue for full kinase activity [27], increased significantly in parallel with α2 AMPK activation (Fig. 2B). Phosphorylation of ACCβ, a known substrate of AMPK [28], also displayed a similar

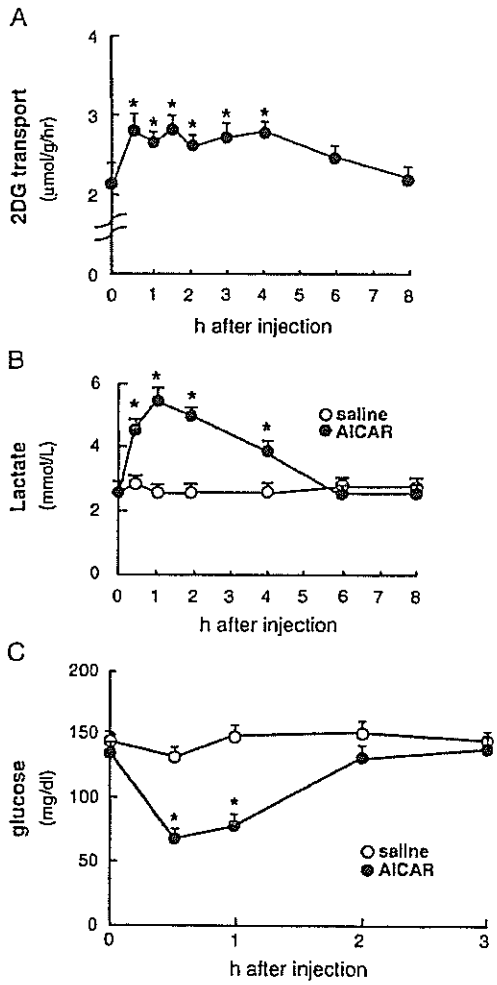

Fig. 3. Time course of 2DG transport activity in soleus muscle (A), blood lactate concentration (B), and blood glucose concentration (C) after subcutaneous injection of AICAR (250 mg/kg). Results are means ± SE (n = 7 to 10 per group). *$P < .05$ compared with basal levels.

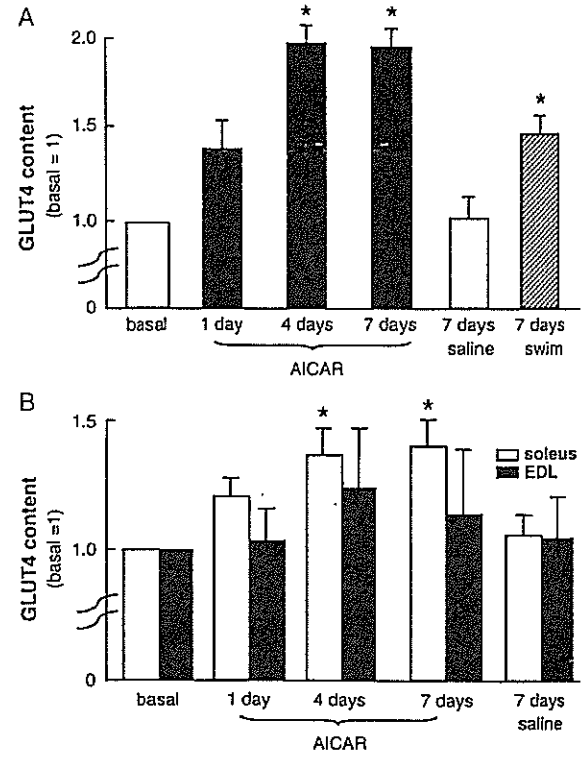

Fig. 4. Glucose transporter 4 protein content in hind limb muscles (A), and soleus and EDL muscles (B). After repeated intraperitoneal injection of AICAR (250 mg/kg) or saline 3 times a day for up to 7 days, or exercise swim training for 7 days, either hind limb or soleus and EDL muscles were isolated, and GLUT4 content was determined with immunoblotting. Results are means ± SE (n = 10 per group). *$P < .05$ compared with basal levels.

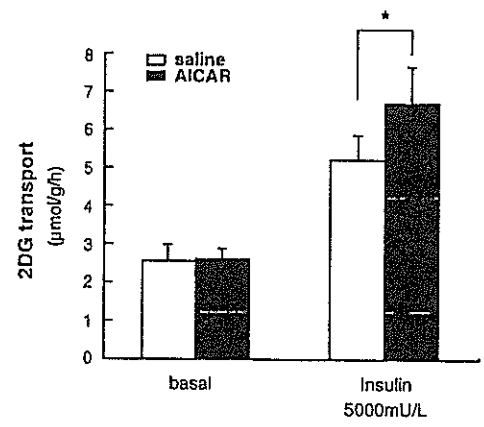

Fig. 5. Basal and insulin-stimulated 2DG transport activity in isolated soleus muscle after repeated intraperitoneal injection of AICAR or saline for 7 days. Soleus muscle was isolated 12 to 16 hours after the last injection, and 2DG transport activity was determined in the absence or presence of 5000 mU/L insulin. Results are means ± SE (n = 7-10 per group). *$P < .05$ compared with the saline group.

pattern as α2 AMPK activity (Fig. 2C). The α2 AMPK activity was significantly elevated for 4 hours after a single intraperitoneal injection of AICAR, whereas the α1 AMPK activity did not change.

3.3. The AICAR-induced increase in 2DG transport activity into skeletal muscle was accompanied by an increase in blood lactate concentration and decrease in blood glucose concentration

In the soleus muscle, a single subcutaneous injection of AICAR increased the rate of 2DG transport by 30%, and this elevated activity was maintained for 4 hours (Fig. 3A). Neither glycogen concentration nor glycogen synthase activity was altered (glycogen: baseline, 36.3 ± 1.6 μmol/g; 0.5 hour, 36.6 ± 0.6 μmol/g; 1.0 hour, 37.9 ± 1.9 μmol/g; 2.0 hours, 38.4 ± 1.3 μmol/g; n = 7-8 per group; glycogen synthase: baseline, 14.9% ± 0.2%; 0.5 hour, 15.2% ± 0.3%; 1.0 hour, 14.4% ± 0.4%; 2.0 hours, 14.6% ± 0.3%; n = 8 per group). In the EDL muscle, 2DG transport did not increase significantly (baseline, 2.0 ± 0.1 μmol/g per hour; 0.5 hour, 2.2 ± 0.1 μmol/g per hour; n = 8 per group, $P < .10$). Blood lactate concentration, an indicator of nonoxidative glucose utilization, was also elevated for 4 hours after injection (Fig. 3B). Blood glucose concentration decreased after a single AICAR injection, and this reduction was abolished within 2 hours after injection (Fig. 3C). Plasma insulin concentration was unchanged at the time points studied (baseline, 1.3 ± 0.3 μg/L; 0.5 hour, 1.3 ± 0.1 μg/L; 1.0 hour, 1.3 ± 0.3 μg/L; 2.0 hours, 1.3 ± 0.3 μg/L; n = 7 per group).

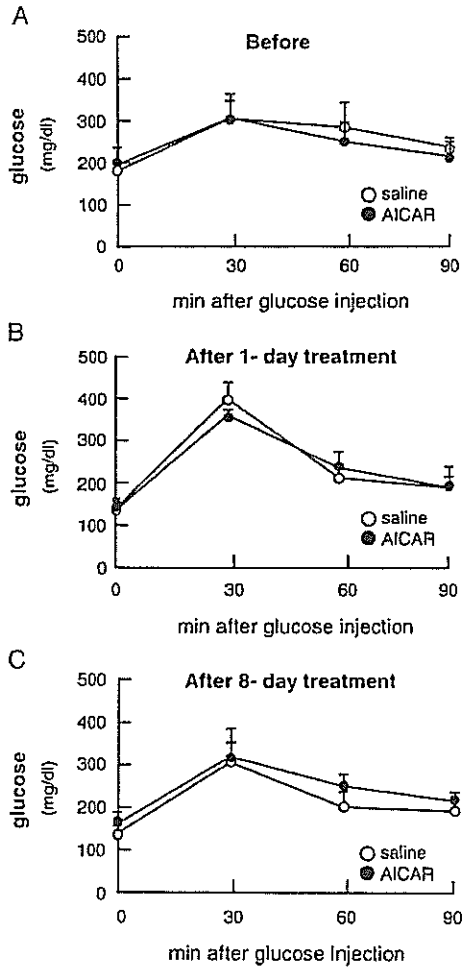

Fig. 6. Glucose tolerance in AICAR- and saline-treated mice. The intraperitoneal GTT was performed before (A) and after repeated intraperitoneal injection of AICAR (250 mg/kg) or saline 3 times a day for 1 day (B) and 8 days (C). Glucose (2.0 g/kg body weight) was administered by intraperitoneal injection 12 to 16 hours after the last injection of AICAR. Results are means ± SE (n = 7-10 per group).

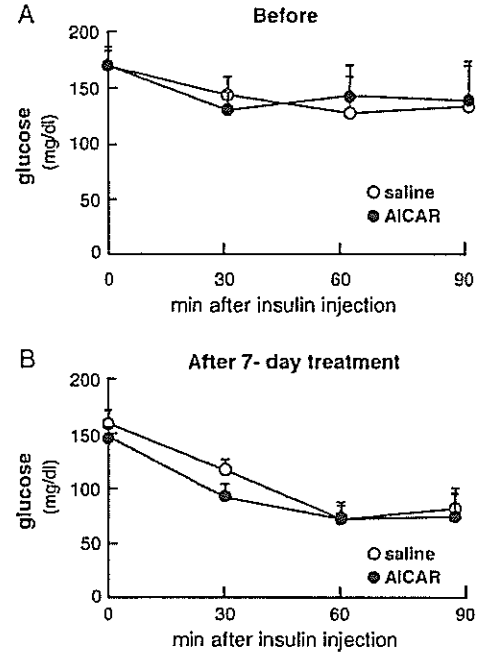

Fig. 7. Insulin tolerance in AICAR- and saline-treated mice. The intraperitoneal ITT was performed before (A) and after (B) repeated intraperitoneal injections of AICAR (250 mg/kg) or saline 3 times a day for 7 days. Glucose (1.2 U/kg body weight) was administered by intraperitoneal injection 12 to 16 hours after the last injection of AICAR. Results are means ± SE (n = 7-10 per group).

3.4. Repeated AICAR injection increased GLUT4 content and insulin-stimulated glucose transport in skeletal muscle

Glucose transporter 4 content in the hind limb muscles increased by 50% after 7 consecutive days of swimming (Fig. 4A). Similarly, repeated intraperitoneal AICAR injection 3 times a day for 4 to 7 days increased GLUT4 content in the hind limb muscles by 90% (Fig. 4A) and in soleus muscle by 40% (Fig. 4B). The increase in GLUT4 in EDL muscle was not significant (Fig. 4B). To determine whether the increased GLUT4 content was associated with enhanced insulin-stimulated glucose transport, we measured 2DG transport activity in soleus muscle treated with AICAR and saline for 7 days. As shown in Fig. 5, the baseline rate of 2DG transport was not affected by AICAR, whereas the

insulin-stimulated rate of 2DG transport activity was 20% higher in AICAR-treated than in saline-treated soleus muscle. In soleus muscle, glycogen synthase activity (% I-form) was not affected (baseline, 14.1% ± 0.3%; 7 days, 14.8% ± 0.8%; n = 8), and glycogen content did not change in response to AICAR treatment (baseline, 39.2 ± 3.1 μmol/g; 7 days, 44.0 ± 3.5 μmol/g; n = 10).

3.5. Whole-body glucose tolerance and insulin tolerance were not affected by repeated AICAR injection

The intraperitoneal GTT (Fig. 6) and ITT (Fig. 7) were performed to determine the effects of repeated AICAR injection on whole-body glucose metabolism. The GTT was performed before (Fig. 6A), after 1 day (Fig. 6B), and after 8 days (Fig. 6C) of administration of AICAR or saline. Glucose concentration did not differ between the AICAR- and saline-treated groups at any time point. Fasting insulin concentration was not affected by the AICAR treatment (baseline, 1.3 ± 0.1; 4 days, 1.2 ± 0.2; 7 days, 1.2 ± 0.2; n = 7). The ITT was performed before (Fig. 7A) and after 7 days (Fig. 7B) of repeated intraperitoneal injection of AICAR or saline. Similar to the results of the GTT, the response to the ITT did not differ significantly between the AICAR- and saline-treated groups. The responses to the GTT (Fig. 8A) and ITT (Fig. 8B) did not differ between sedentary animals and those exercised for 7 days. Body weight was unchanged after AICAR administration (baseline, 24.2 ± 0.6 g; 7 days, 24.4 ± 0.4 g; n = 10).

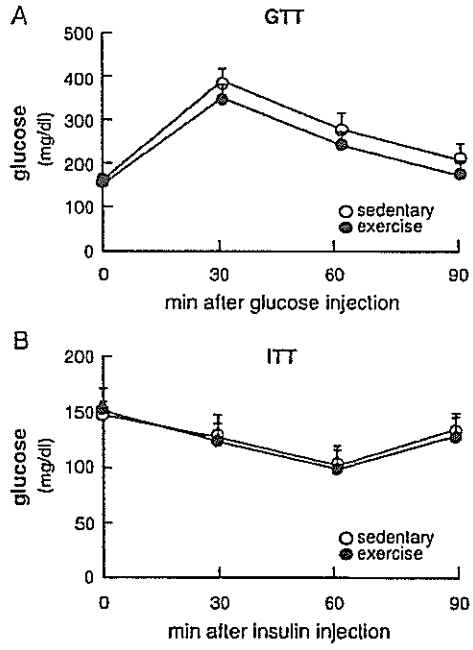

Fig. 8. Glucose tolerance and insulin tolerance in sedentary and exercise-trained mice. The exercise group swam for 30 minutes twice a day for 7 days. The intraperitoneal GTT (A) and intraperitoneal ITT (B) were performed 16 hours after the last bout of exercise. Results are means ± SE (n = 7-10 per group).

4. Discussion

Endurance exercise activates predominantly α2 AMPK in human and animal skeletal muscles. Fujii et al [17] reported a 2-fold increase in α2 AMPK activity in human vastus lateralis muscle after 60-minute cycle exercise at 70% $\dot{V}O_2$max, but no change in α1 AMPK after exercise. Similarly, Wojtaszewski et al [18] reported a 3-fold activation of α2 AMPK in human vastus lateralis after cycle exercise at 75% $\dot{V}O_2$max for 55 minutes followed by 90% $\dot{V}O_2$max for 5 minutes. Musi et al [8] showed that α2 AMPK is activated by 50% to 100% after treadmill running (18-32 m/min at 10% grade for 1 hour) and that this activation is accompanied by a significant increase in 3-*O*-methylglucose transport in rat epitrochlearis muscle. Our observations of a 2-fold increase in α2 AMPK activity after 30-minute swimming at ~60% $\dot{V}O_2$max in mouse skeletal muscle, but no increase in α1 AMPK activity, are consistent with these previous findings.

We administered 250 mg/kg AICAR subcutaneously or intraperitoneally to activate α2 AMPK to the same extent as the activation observed in skeletal muscle after exercise. AICAR is taken up into skeletal muscle and metabolized by adenosine kinase to form ZMP, a monophosphorylated derivative that mimics the effects of AMP on AMPK without changing the intracellular levels of AMP or ATP [29]. The concentration of intracellular AMP and the AMP/ATP ratio are both important determinants of AMPK activity; α2 AMPK has greater dependence on AMP than the α1 isoform in both the allosteric activation by AMP and the covalent activation by upstream kinase [27,30]. In our study, both types of injections activated α2 AMPK in skeletal muscle, but the intraperitoneal injection produced a longer-lasting activation than the subcutaneous injection. α2 AMPK activity increased for at least 4 hours after the intraperitoneal injection, but the enzyme activity returned to baseline within 2 hours after subcutaneous injection. Although the precise mechanism by which AICAR activates α2 AMPK is unknown, the site of injection may have a substantial influence on the rate of absorption, and the time course and intensity of activation.

Although AICAR is not strictly specific for AMPK [31-33], recent studies with AICAR have provided important information about the function of AMPK in muscle glucose transport and GLUT4 expression. Mu et al [7] selectively blocked AMPK in mouse skeletal muscle with muscle-specific expression of a dominant-negative, kinase-dead form of α2 AMPK. In this mouse, the stimulatory effects of AICAR on glucose transport [7] and GLUT4 expression [15] were blocked completely. In addition, the AICAR-stimulated glucose transport was abolished in skeletal muscles from whole-body α2 knockout mouse, but not in muscles from whole-body α1 knockout mouse [9]. Furthermore, incubating isolated animal muscles in the presence of AICAR increased glucose transport [4,34] and GLUT4 protein expression [11]. These results strongly

indicate that the metabolic effects of AICAR on skeletal muscle involve α2 AMPK-dependent signaling events, which can occur independent of changes in systemic factors. Interestingly, in mice with muscle-specific expression of a dominant-negative, kinase-dead AMPK, glucose transport is only partially reduced in response to electrically stimulated contractions of hind limb muscles [7], and muscle GLUT4 messenger RNA increases after endurance exercise (two 3-hour bouts of treadmill running) [15]. Similarly, the rate of glucose transport increases after electrical stimulation of isolated muscles from the transgenic mouse expressing the dominant-negative α2 AMPK [9]. Although the previous studies did not examine the effects of moderate-intensity exercise, there may be additional signaling mechanisms, other than α2 AMPK, leading to exercise-induced metabolic events in skeletal muscle.

We found that the α2 AMPK activity decreased within 2 hours after subcutaneous injection of AICAR (Fig. 2A), whereas 2DG transport remained elevated for at least 4 hours (Fig. 3A). Musi et al [8] previously demonstrated that the time course of AMPK is dissociated from the glucose transport activities in isolated rat epitrochlearis muscle during in vitro electrical stimulation of muscle contractions. AMPK activity decreased rapidly after the cessation of tetanic contractions ($t_{1/2}$ = 8 minutes), whereas the rate of decrease in 3-*O*-methylglucose transport was much slower and had decreased by only 48% after 60 minutes. This previous report and our findings suggest that, although AMPK may be involved in stimulating glucose transport, sustained AMPK activity is not required to maintain transport activity.

Activation of AMPK and its effects vary by muscle fiber type. In the studies using rat skeletal muscle, long-term AICAR administration has the greatest effects on GLUT4 and glycogen content in fast-twitch muscles [10,12,35]. Daily subcutaneous injections of AICAR at a dose of 1 g/kg body weight for 4 weeks increased GLUT4 and glycogen content in the red and white quadriceps, but not in the soleus muscle in rats [35]. Moreover, acute AICAR exposure stimulates glucose transport in white muscles, but has no effect in rat soleus muscle [34,36]. In contrast, incubation with AICAR markedly increases glucose transport in both soleus and EDL muscles in the mouse [34]. We also found significant increases in 2DG transport activity and GLUT4 content ($P < .05$) in mouse soleus muscle. This discrepancy in the effects of AICAR between rat and mouse soleus muscles may be due to a greater percentage of fast-twitch muscle fibers within mouse soleus (ie, the mouse soleus has proportionately more fast-twitch fibers than the rat soleus) [34]. Because of the nonspecific stimulation by AICAR in mouse skeletal muscle, we believe that most skeletal muscles responded to the subcutaneous and intraperitoneal AICAR administration in our study.

The concept that a large number of skeletal muscles are stimulated by AICAR in mouse is indirectly supported by our observation that AICAR treatment caused a marked increase in blood lactate concentration and reduction in blood glucose concentration, with a corresponding increase in glucose transport activity (Fig. 3). The hypoglycemic effect of AICAR is blunted in mice with muscle-specific expression of the dominant negative AMPK [7], emphasizing the pivotal role of muscle AMPK in AICAR-induced hypoglycemia. However, it has also been reported that, after the conversion into ZMP, AICAR exerts a dose-dependent inhibition of fructose-1,6-bisphosphatase, which inhibits gluconeogenesis and enhances lactate production in the liver [32,33]. Thus, the effects on both skeletal muscle and other tissues, including liver, may contribute to the hypoglycemia and elevated lactate concentrations caused by AICAR.

The contribution of increased muscle GLUT4 to glucose tolerance and insulin sensitivity has been clearly documented in studies using transgenic mice with muscle-specific overexpression of GLUT4 [37,38]. However, we found that AICAR treatment had no effect on blood glucose excursions during the GTT and ITT compared with the saline treatment (Figs. 6 and 7). Similarly, swimming exercise for 7 days did not affect glucose excursions compared with sedentary mice (Fig. 8). Although the underlying mechanism is unclear, the effects of long-term AICAR treatment and swimming exercise may be below the detectable limit of the GTT or ITT because we used the metabolically normal mouse (C57/B6). This concept is consistent with the observation that metabolic improvements occurred after 7 days of treatment with AICAR and were detected by the oral GTT (3 mg/kg) and ITT (10 U/kg) in KKA^y-CETP mice, a model of insulin-resistant type 2 diabetes mellitus [39]. Because we performed ITTs on fed animals, the food consumption of the animals coming into the test could affect the response, and there may have been a different response at 15-minute time point that returned to control at 30 minutes in GTTs.

In summary, we found that pharmacological activation of α2AMPK by AICAR at a physiological level led to a short-term increase in glucose transport and that long-term activation of the isoform increased GLUT4 protein and enhanced insulin-stimulated glucose transport in mouse skeletal muscle. These results strongly suggest that activation of α2 AMPK during moderate exercise plays pivotal roles in exercise-stimulated glucose uptake and utilization in skeletal muscle. Our data also support the hypothesis that α2 AMPK can be a target of pharmacological manipulation aiming to improve glucose metabolism in skeletal muscle.

Acknowledgment

This study was supported by a grant from the Japanese Ministry of Education, Science, Sports, and Culture (15500441).

We are grateful to Laurie J. Goodyear and Nobuharu Fujii for suggestions. We thank Wataru Mizunoya and Shinici

Oyaizu, for technical assistance. We also thank Yoko Koyama and Kaoru Ijiri for secretarial assistance.

References

[1] Hayashi T, Wojtaszewski JF, Goodyear LJ. Exercise regulation of glucose transport in skeletal muscle. Am J Physiol 1997;273: E1039-51.

[2] MacLean PS, Zheng D, Dohm GL. Muscle glucose transporter (GLUT 4) gene expression during exercise. Exerc Sport Sci Rev 2000;28:148-52.

[3] Etgen Jr GJ, Jensen J, Wilson CM, et al. Exercise training reverses insulin resistance in muscle by enhanced recruitment of GLUT-4 to the cell surface. Am J Physiol 1997;272:E864-9.

[4] Hayashi T, Hirshman MF, Kurth EJ, et al. Evidence for 5' AMP-activated protein kinase mediation of the effect of muscle contraction on glucose transport. Diabetes 1998;47:1369-73.

[5] Kurth-Kraczek EJ, Hirshman MF, Goodyear LJ, et al. 5'AMP-activated protein kinase activation causes GLUT4 translocation in skeletal muscle. Diabetes 1999;48:1667-71.

[6] Hayashi T, Hirshman MF, Fujii N, et al. Metabolic stress and altered glucose transport: activation of AMP-activated protein kinase as a unifying coupling mechanism. Diabetes 2000;49:527-31.

[7] Mu J, Brozinick Jr JT, Valladares O, et al. A role for AMP-activated protein kinase in contraction- and hypoxia-regulated glucose transport in skeletal muscle. Mol Cell 2001;7:1085-94.

[8] Musi N, Hayashi T, Fujii N, et al. AMP-activated protein kinase activity and glucose uptake in rat skeletal muscle. Am J Physiol Endocrinol Metab 2001;280:E677-84.

[9] Jorgensen SB, Viollet B, Andreelli F, et al. Knockout of the alpha2 but not alpha1 5'-AMP–activated protein kinase isoform abolishes 5-aminoimidazole-4-carboxamide-1-beta-4-ribofuranosidebut not contraction-induced glucose uptake in skeletal muscle. J Biol Chem 2004;279:1070-9.

[10] Holmes BF, Kurth-Kraczek EJ, Winder WW. Chronic activation of 5'-AMP–activated protein kinase increases GLUT-4, hexokinase, and glycogen in muscle. J Appl Physiol 1999;87:1990-5.

[11] Ojuka EO, Nolte LA, Holloszy JO. Increased expression of GLUT-4 and hexokinase in rat epitrochlearis muscles exposed to AICAR in vitro. J Appl Physiol 2000;88:1072-5.

[12] Buhl ES, Jessen N, Schmitz O, et al. Chronic treatment with 5-aminoimidazole-4-carboxamide-1-beta-D-ribofuranoside increases insulin-stimulated glucose uptake and GLUT4 translocation in rat skeletal muscles in a fiber type–specific manner. Diabetes 2001;50:12-7.

[13] Zheng D, MacLean PS, Pohnert SC, et al. Regulation of muscle GLUT-4 transcription by AMP-activated protein kinase. J Appl Physiol 2001;91:1073-83.

[14] MacLean PS, Zheng D, Jones JP, et al. Exercise-induced transcription of the muscle glucose transporter (GLUT 4) gene. Biochem Biophys Res Commun 2002;292:409-14.

[15] Holmes BF, Lang DB, Birnbaum MJ, et al. AMP kinase is not required for the GLUT4 response to exercise and denervation in skeletal muscle. Am J Physiol Endocrinol Metab 2004;287:E739-43.

[16] Stapleton D, Mitchelhill KI, Gao G, et al. Mammalian AMP-activated protein kinase subfamily. J Biol Chem 1996;271:611-4.

[17] Fujii N, Hayashi T, Hirshman MF, et al. Exercise induces isoform-specific increase in 5'AMP-activated protein kinase activity in human skeletal muscle. Biochem Biophys Res Commun 2000;273:1150-5.

[18] Wojtaszewski JF, Nielsen P, Hansen BF, et al. Isoform-specific and exercise intensity-dependent activation of 5'-AMP–activated protein kinase in human skeletal muscle. J Physiol 2000;528(Pt 1):221-6.

[19] Stephens TJ, Chen ZP, Canny BJ, et al. Progressive increase in human skeletal muscle AMPKalpha2 activity and ACC phosphorylation during exercise. Am J Physiol Endocrinol Metab 2002;282:E688-94.

[20] Musi N, Fujii N, Hirshman MF, et al. AMP-activated protein kinase (AMPK) is activated in muscle of subjects with type 2 diabetes during exercise. Diabetes 2001;50:921-7.

[21] Chen ZP, McConell GK, Michell BJ, et al. AMPK signaling in contracting human skeletal muscle: acetyl-CoA carboxylase and NO synthase phosphorylation. Am J Physiol Endocrinol Metab 2000;279:E1202-6.

[22] Matsumoto K, Ishihara K, Tanaka K, et al. An adjustable-current swimming pool for the evaluation of endurance capacity of mice. J Appl Physiol 1996;81:1843-9.

[23] Masuzaki H, Ogawa Y, Aizawa-Abe M, et al. Glucose metabolism and insulin sensitivity in transgenic mice overexpressing leptin with lethal yellow agouti mutation: usefulness of leptin for the treatment of obesity-associated diabetes. Diabetes 1999;48:1615-22.

[24] Toyoda T, Hayashi T, Miyamoto L, et al. Possible involvement of the alpha1 isoform of 5' AMP-activated protein kinase in oxidative stress-stimulated glucose transport in skeletal muscle. Am J Physiol Endocrinol Metab 2004;287:E166-73.

[25] Bruning JC, Michael MD, Winnay JN, et al. A muscle-specific insulin receptor knockout exhibits features of the metabolic syndrome of NIDDM without altering glucose tolerance. Mol Cell 1998;2:559-69.

[26] Hayashi T, Hirshman MF, Dufresne SD, et al. Skeletal muscle contractile activity in vitro stimulates mitogen-activated protein kinase signaling. Am J Physiol 1999;277:C701-7.

[27] Stein SC, Woods A, Jones NA, et al. The regulation of AMP-activated protein kinase by phosphorylation. Biochem J 2000;3:437-43.

[28] Davies SP, Sim AT, Hardie DG. Location and function of three sites phosphorylated on rat acetyl-CoA carboxylase by the AMP-activated protein kinase. Eur J Biochem 1990;187:183-90.

[29] Hardie DG, Carling D. The AMP-activated protein kinase—fuel gauge of the mammalian cell? Eur J Biochem 1997;246:259-73.

[30] Salt I, Celler JW, Hawley SA, et al. AMP-activated protein kinase: greater AMP dependence, and preferential nuclear localization, of complexes containing the alpha2 isoform. Biochem J 1998;334 (Pt 1):177-87.

[31] Young ME, Radda GK, Leighton B. Activation of glycogen phosphorylase and glycogenolysis in rat skeletal muscle by AICAR—an activator of AMP-activated protein kinase. FEBS Lett 1996;382:43-7.

[32] Vincent MF, Erion MD, Gruber HE, et al. Hypoglycaemic effect of AICAriboside in mice. Diabetologia 1996;39:1148-55.

[33] Vincent MF, Marangos PJ, Gruber HE, et al. Inhibition by AICA riboside of gluconeogenesis in isolated rat hepatocytes. Diabetes 1991;40:1259-66.

[34] Balon TW, Jasman AP. Acute exposure to AICAR increases glucose transport in mouse EDL and soleus muscle. Biochem Biophys Res Commun 2001;282:1008-11.

[35] Winder WW, Holmes BF, Rubink DS, et al. Activation of AMP-activated protein kinase increases mitochondrial enzymes in skeletal muscle. J Appl Physiol 2000;88:2219-26.

[36] Ai H, Ihlemann J, Hellsten Y, et al. Effect of fiber type and nutritional state on AICAR- and contraction-stimulated glucose transport in rat muscle. Am J Physiol Endocrinol Metab 2002;282: E1291-300.

[37] Leturque A, Loizeau M, Vaulont S, et al. Improvement of insulin action in diabetic transgenic mice selectively overexpressing GLUT4 in skeletal muscle. Diabetes 1996;45:23-7.

[38] Tsao TS, Burcelin R, Katz EB, et al. Enhanced insulin action due to targeted GLUT4 overexpression exclusively in muscle. Diabetes 1996;45:28-36.

[39] Fiedler M, Zierath JR, Selen G, et al. 5-Aminoimidazole-4-carboxy-amide-1-beta-D-ribofuranoside treatment ameliorates hyperglycaemia and hyperinsulinaemia but not dyslipidaemia in KKAy-CETP mice. Diabetologia 2001;44:2180-6.

Altered Gene Expression Related to Glomerulogenesis and Podocyte Structure in Early Diabetic Nephropathy of *db/db* Mice and Its Restoration by Pioglitazone

Hisashi Makino, Yoshihiro Miyamoto, Kazutomo Sawai, Kiyoshi Mori, Masashi Mukoyama, Kazuwa Nakao, Yasunao Yoshimasa, and Shin-ichi Suga

Original Article

Altered Gene Expression Related to Glomerulogenesis and Podocyte Structure in Early Diabetic Nephropathy of *db/db* Mice and Its Restoration by Pioglitazone

Hisashi Makino,[1] Yoshihiro Miyamoto,[1] Kazutomo Sawai,[2] Kiyoshi Mori,[2] Masashi Mukoyama,[2] Kazuwa Nakao,[2] Yasunao Yoshimasa,[1] and Shin-ichi Suga[3]

Glomerular injury plays a pivotal role in the development of diabetic nephropathy. To elucidate molecular mechanisms underlying diabetic glomerulopathy, we compared glomerular gene expression profiles of *db/db* mice with those of *db/m* control mice at a normoalbuminuric stage characterized by hyperglycemia and at an early stage of diabetic nephropathy with elevated albuminuria, using cDNA microarray. In *db/db* mice at the normoalbuminuric stage, hypoxia-inducible factor-1α (HIF-1α), ephrin B2, glomerular epithelial protein 1, and Pod-1, which play key roles in glomerulogenesis, were already upregulated in parallel with an alteration of genes related to glucose metabolism, lipid metabolism, and oxidative stress. Podocyte structure-related genes, actinin 4α and dystroglycan 1 (DG1), were also significantly upregulated at an early stage. The alteration in the expression of these genes was confirmed by quantitative RT-PCR. Through pioglitazone treatment, gene expression of ephrin B2, Pod-1, actinin 4α, and DG1, as well as that of oxidative stress and lipid metabolism, was restored concomitant with attenuation of albuminuria. In addition, HIF-1α protein expression was partially attenuated by pioglitazone. These results suggest that not only metabolic alteration and oxidative stress, but also the alteration of gene expression related to glomerulogenesis and podocyte structure, may be involved in the pathogenesis of early diabetic glomerulopathy in type 2 diabetes. *Diabetes* 55:2747–2756, 2006

Diabetic nephropathy is the leading cause of end-stage renal disease in the U.S., Japan, and most of Europe (1). Clinical features of diabetic nephropathy are development of albuminuria followed by persistent proteinuria and, later, reduction of glomerular filtration rate (2). Increased thickness of glomerular basement membrane and augmentation of glomerular extracellular matrix are recognized as pathological hallmarks of diabetic nephropathy (2). Thus, glomerular injury is apparently critical for the initiation and progression of the disease. Several pathways are postulated as potential mechanisms of diabetic nephropathy, including renal hemodynamic changes, accretion of advanced glycation end products, intracellular accumulation of sorbitol, oxidation of glycoproteins by reactive oxygen species, and activation of protein kinase C (2,3). Recently, much attention has been paid to the role of podocyte injury in glomerular diseases, including diabetic nephropathy (3–6). However, the precise molecular mechanisms underlying diabetic glomerulopathy still remain unclear.

Microarray is a novel tool by which whole-genome analysis can identify new genes and pathways that are important for the pathophysiology of diabetic nephropathy (7). Although several laboratories recently performed cDNA microarray analyses of diabetic kidney (8–12), most of them examined gene expression of whole kidney, despite the importance of glomerular injury in diabetic nephropathy. In addition, analysis of whole kidney often makes it difficult to select genes associated with diabetic glomerulopathy because glomeruli occupy only a small part of the kidney. Only one of these reports showed the gene expression profile of glomeruli (12). However, because the report analyzed glomeruli from advanced diabetic nephropathy patients with apparent histological changes, it did not provide much information about the mechanism of early diabetic glomerulopathy.

In this study, we performed microarray analysis using isolated glomeruli from diabetic mice at a normoalbuminuric stage and an early stage of diabetic nephropathy with no apparent histological change in order to find the genes that are strongly associated with diabetic glomerular injury. This approach also enabled us to avoid the modification of gene expression profiles by cell component alteration. We analyzed *db/db* mice, a genetic model of type 2 diabetes with obesity and insulin resistance (13), because they exhibited histological changes resembling those in human diabetic nephropathy (13,14). Because accumulating evidence indicates that insulin resistance participates in the pathogenesis of diabetic nephropathy in type 2 diabetes (15), we also examined the effects of pioglitazone, one of the insulin sensitizers that improves insulin sensitivity, on the gene expression profile of *db/db* mice.

RESEARCH DESIGN AND METHODS

Male diabetic *db/db* mice and their nondiabetic *db/m* littermates were used for this study. All mice were purchased from CLEA Japan (Tokyo). These *db/db*

From the [1]Department of Atherosclerosis and Diabetes, National Cardiovascular Center, Suita City, Osaka, Japan; the [2]Department of Endocrinology and Metabolism, Kyoto University Graduate School of Medicine, Kyoto, Japan; and the [3]National Cardiovascular Center Research Institute, Suita City, Osaka, Japan.

Address correspondence and reprint requests to Shin-ichi Suga, MD, PhD, National Cardiovascular Center Research Institute, 5-7-1 Fujishiro-dai, Suita City, Osaka 565-8565, Japan. E-mail: s-suga@umin.ac.jp.

Received for publication 27 December 2005 and accepted in revised form 27 June 2006.

DG1, dystroglycan 1; GLEPP1, glomerular epithelial protein 1; HIF-1α, hypoxia-inducible factor-1α; VEGF, vascular endothelial growth factor.

DOI: 10.2337/db05-1683

TABLE 1
Characteristics of experimental animals

	5 weeks	7 weeks
Body weight (g)		
db/m	21.5 ± 0.4	25.4 ± 0.3
db/db	22.8 ± 0.7	37.1 ± 0.3*
Blood glucose levels (mg/dl)		
db/m	182 ± 6	128 ± 12
db/db	238 ± 17†	575 ± 25*
Urinary albumin excretion (μg/16 h)		
db/m	8.9 ± 1.5	5.2 ± 1.1
db/db	12.2 ± 1.3	32.5 ± 6.3*
Urinary albumin excretion (μg/mg creatine)		
db/m	0.29 ± 0.06	0.16 ± 0.02
db/db	0.19 ± 0.07	0.49 ± 0.13*

Data are the means ± SE. Each group has $n = 12$. *$P < 0.01$, †$P < 0.05$ vs. *db/m*.

mice began to show hyperglycemia at 5 weeks of age and a significant increase in urinary albumin excretion at 7 weeks of age (Table 1). Mice were killed under pentobarbital anesthesia at 5 and 7 weeks of age to obtain kidney samples for isolation of glomeruli and immunohistochemistry.

To study the role of insulin resistance in the development of diabetic nephropathy, we administered pioglitazone (Takeda Pharmaceutical, Osaka, Japan), a peroxisome proliferator–activated receptor-γ agonist, to two other groups of 5-week-old *db/db* mice for 2 weeks ($n = 12$ in each). Pioglitazone was mixed with normal mouse chow and administered at a dose of 3 or 15 mg · kg body wt^{-1} · day^{-1} because 15 mg/kg of pioglitazone was reported to improve insulin sensitivity in *db/db* mice (16).

We obtained 16-h urine specimens from all mice at 5 and 7 weeks of age for the measurement of albumin excretion (17). Urinary albumin excretion was determined by enzyme-linked immunosorbent assay (Albuwell; Exocell, Philadelphia, PA) (17). Urinary creatinine levels were measured by enzymatic method (SRL, Tokyo) (17). For the insulin tolerance test, mice were fasted for 6 h and given 1.25 unit/kg i.p. human regular insulin (Novo Nordisk, Bagsvaerd, Denmark) (18).

Isolation of glomeruli. We prepared two isolated glomerular samples from each group. An isolated glomerular sample was obtained from the kidneys of six mice by differential sieving method, using mesh diameters of 45, 75, and 150 μm (19). The purity of each sample was confirmed by microscopy. The glomerular samples were ~80% pure on average, and there was no difference in purity among the samples.

Microarray gene expression. Total RNA was extracted from glomerular samples by the acid guanidine-phenol-chloroform method, using Trizol reagent (Life Technologies) (20). We essentially followed the procedures described in detail in the GeneChip expression analysis manual (Affymetrix, Santa Clara, CA). In brief, 10 μg of total RNA was used for cDNA synthesis (Superscript II kit; Life Technologies, Rockville, MD). Biotin-labeled cRNA was produced through in vitro transcription of cDNA, using an ENZO BioArray high-yield RNA transcript labeling kit (Affymetrix). Fragmented cRNA (15 μg) was hybridized to an Affymetrix Murine Genome U74Av2 GeneChip at 45°C for 16 h. The samples were stained and washed according to the manufacturer's protocol on a Fluidics Station 400 (Affymetrix) and scanned on a GeneArray scanner (Affymetrix) (8,21).

Primary data extraction was performed with Microarray Suite 5.0 (Affymetrix) because analysis by Microarray Suite 5.0 is more reliable than other methods (22). Microarray Suite 5.0 software normalized the data of each microarray and compared the expression between the two different arrays. Moreover, the software could determine statistically whether each gene was present (reliably detected) or absent (not detected) in one array and whether each gene increased or decreased between two different arrays. Signal normalization across samples was carried out, using all probe sets, with a mean expression value of 500 (8,21). To allow comparisons between any two experiments, pairwise comparisons were made between *db/m* and *db/db* mice by Microarray Suite 5.0. Because two arrays were used for each group (*db/m* 1, *db/m* 2, *db/db* 1, and *db/db* 2), we performed four comparison analyses (i.e., *db/m* 1 vs. *db/db* 1, *db/m* 1 vs. *db/db* 2, *db/m* 2 vs. *db/db* 1, and *db/m* 2 vs. *db/db* 2). Genes showing an increased or decreased call in at least three of four comparisons were defined as genes showing a significant change. As an internal control, we chose GAPDH and confirmed that there was no difference in GAPDH expression level between each sample in microarray analysis.

Podocyte culture. Cultivation of conditionally immortalized mouse podocytes (a gift from Dr. Peter Mundel, Albert Einstein College of Medicine, Bronx, NY) was performed as reported previously (23). Briefly, cells were grown on a type 1 collagen–coated dish (IPC-03; Koken, Tokyo) at 33°C in the presence of 10 units/ml murine γ-interferon (Life Technologies, Gaithersburg, MD) in RPMI 1640 medium (Nihonseiyaku, Tokyo) supplemented with 10% FCS (Cansera International, Etobicoke, ON, Canada) and antibiotics. To induce differentiation, podocytes were maintained at 37°C without interferon. Before the experiment, cells were differentiated for 2 weeks without passage, followed by culture in RPMI 1640 containing 1% FCS supplemented with 5.6 mmol/l glucose (normal glucose) or 25 mmol/l glucose (high glucose) for 14 days.

Quantitative RT-PCR. We reverse transcribed 2.5 μg of total RNA using Ready-To-Go (Amersham Pharmacia Biotech, Piscataway, NJ) (20). TaqMan real-time quantitative PCR was performed and analyzed according to the manufacturer's instructions (Applied Biosystems, Foster City, CA) (24). Primers and probe sequences were selected by using Primer Express (Applied Biosystems). GAPDH was used for internal control because its expression level did not show a significant difference between *db/m* and *db/db* in our microarray analysis.

Immunohistochemistry. Kidneys were dissected immediately and fixed in 10% formalin, embedded in paraffin, and sectioned at 4 μm. Hypoxia-inducible factor-1α (HIF-1α) was identified with monoclonal IgG HIF-1α antibody 67 (Novus Biological, Littleton, CO) at a 1:2000 dilution, using the Tyramide signal amplification system (PerkinElmer Life Sciences, Boston, MA) (25). The number of HIF-1α–positive cells was counted in 30 randomly selected glomeruli in the outer cortex.

Statistical analyses. Data are the means ± SE. Statistical analyses were performed using ANOVA followed by Scheffe's test. $P < 0.05$ was considered statistically significant.

RESULTS

Characteristics of *db/db* mice. At 5 weeks of age, *db/db* mice already showed significant hyperglycemia, whereas urinary albumin excretion did not increase compared with *db/m* mice (Table 1). There was no difference in renal histology between *db/m* and *db/db* mice at 5 weeks of age under light microscopic observation. At 7 weeks of age, *db/db* mice showed significant elevation of urinary albumin excretion (Table 1). However, no apparent histological difference was observed between *db/db* and *db/m* mice (data not shown). Thus, 5-week-old *db/db* mice exhibited features similar to the human normoalbuminuric stage, and 7-week-old mice showed features similar to the human early stage of diabetic nephropathy.

Comparison analysis of gene expression profiles between *db/db* and *db/m* mice. Table 2 shows 134 genes with an absolute relative log ratio >0.5 and showing significant change by Microarray Suite 5.0 analysis at 5 and/or 7 weeks of age. At 5 weeks of age, 105 genes were differentially expressed (65 increased, 40 decreased) between *db/db* and *db/m* mouse glomeruli. Among them, there were genes related to oxidative stress, glucose metabolism, lipid metabolism, cell growth, fibrosis, apoptosis, vasoactive mediators, calcium-binding proteins, coagulation, cell structure, and extracellular matrix components. We also observed significant differences in the expression of development-related genes, including several genes related to kidney development. At 7 weeks of age, 116 genes expressed differentially (72 increased, 44 decreased) between *db/db* and *db/m* mouse glomeruli. In addition to the genes showing differential expression at 5 weeks of age, genes related to cell structure, particularly podocyte structure, and solute carrier family were expressed differentially between *db/db* and *db/m*.

We next confirmed the differential expression of genes by quantitative real-time RT-PCR. Because glomerular response to injury is accompanied by activation of the development-related genes (26), we measured mRNA levels of kidney development–related genes, i.e., ephrin B2

TABLE 2
Genes up- or downregulated in *db/db* mice at 5 and 7 weeks of age

Gene	ID	Fold change of genes up- or downregulated in *db/db* mice compared with *db/m*		Fold change of genes up- or downregulated in pioglitazone-treated *db/db* mice	
		5 weeks	7 weeks	Pioglitazone 3 mg/kg	Pioglitazone 15 mg/kg
Oxidative stress related					
Upregulated					
Glutathione-S-transferase α2	J03958	7.77*	9.49*	10.70	0.95†
Cytochrome P450 4a14	Y11638	6.52*	15.26*	9.76	0.76†
Cytochrome c oxidase subunit VIa	U08439	2.17*	14.90*	9.68	2.99
Glutathione S transferase ω1	AI843119	1.87*	1.73*	2.16	0.81†
Glutathione S transferase ω1	AI843119	1.87*	1.73*	2.16	0.81†
Glutathione S transferase θ1	X98055:	1.73*	1.52*	1.90	1.02
Metallothionein 1	V00835	1.61*	2.79*	4.7	1.14†
Calcipressin	AI846152	1.61	2.92*	2.16	1.26†
Cytochrome P450 4a10	AB018421	1.57*	2.34*	1.73	0.82†
Antioxidant enzyme AOE372	U96746	1.31	1.91*	1.58	0.90†
Downregulated					
Cysteine sulfinic acid decarboxylase	AW120896	0.31*	0.56*	0.48	1.06†
Cytochrome P450 2e1	X01026	0.43*	0.37	0.43	0.91†
Cytochrome P450 2a4	M19319	0.45*	0.32*	0.22	0.87†
Malic enzyme supernatant	J02652	0.48*	0.41*	0.51	1.11†
Glutamate cysteine ligase	U95053	0.50*	0.53*	0.34	0.96†
Extracellular superoxide dismutase	U38261	0.60*	0.70*	0.70	1.50†
Peroxisomal acyl-CoA oxidase	AF006688	0.74	0.56*	0.72	1.02†
Lipid metabolism related					
Upregulated					
Apolipoprotein E	D00466	3.00*	3.32*	4.98	1.16†
Stearoyl-coenzyme A desaturase 2	M26270	2.34*	2.06*	3.09	1.26†
Thioredoxin interacting protein	AI839138	1.96*	1.3	1.43	1.17
Oxysterol-binding protein like 5	AW121299	1.78*	1.41	2.15	1.09
Phosphatidic acid phosphatase 2b	AI847054	1.65*	0.95	2.93	2.10
Acetyl coenzyme A acyltransferase 2	AI849271	1.28*	1.82*	1.91	0.89†
Sterol-C4 methyl oxidase like	AI848668	1.13	2.06*	2.39	2.06
Acetyl-coenzyme A synthetase 2	AW125884	1.19	1.65*	2.16	0.99
Downregulated					
Lipoprotein lipase	M63335	0.13*	0.17*	0.09	0.93†
Alcohol dehydrogenase class I gene	M22679	0.22*	0.23*	0.21	1.08†
Degenerative spermatocyte homolog 2	AI852933	0.27*	0.25*	0.24	0.97†
α-Methylacyl-CoA racemace	U89906	0.36*	0.28*	0.37	0.98†
Diphosphate δ isomerase	AA716963	0.36*	0.35*	0.27	0.91†
Enoyl-coenzyme A hydratase	AJ011864	0.46*	0.43*	0.22	1.23†
Coenzyme A synthase	AI837229	0.53*	0.36*	0.29	0.88†
Fatty acid transporter protein 2	AF072757	0.68	0.54*	0.49	0.89†
Lysophospholipase 1	AA840463	0.72	0.61*	0.29	0.81
Cell growth related					
Upregulated					
Dual-specificity phosphatase 1	X61940	2.30*	0.90	1.31	0.86
Cysteine-rich protein 1	D88793	2.06*	1.91*	2.90	1.64
Prothymosin β4	U38967	2.01*	1.57*	1.60	1.16
Calpactin I heavy chain (p36)	M14044	1.96*	1.31	2.04	1.18
Cyclin-dependent kinase inhibitor 1C	U22399	1.96*	1.25	1.95	1.39
Nuclear protein 1	AI852641	1.75*	2.11*	3.84	1.56
Minopontin	X13986	1.73*	2.93*	3.25	0.94†
Annexin A1	:AV003419	1.73*	1.15	2.62	1.15
Biglycan	X53928	1.65*	1.45	2.64	1.38
Cyclin-dependent protein kinase	AI849556	1.69	2.01*	2.23	1.17†
CDC28 protein kinase regulatory subunit 2	AA681998	1.19	1.96*	1.55	1.06†
Downregulated					
Sin3-associated protein (sap 30)	AF075136	0.48*	0.36*	0.25	0.76†
Ornithine decarboxylase	M12330	0.56*	0.37*	0.43	1.16†
FK506BP-rapamycin–associated protein 1	AI853977	0.58*	0.45*	0.70†	1.11†

Continued on following page

TABLE 2
Continued

Gene	ID	Fold change of genes up- or downregulated in *db/db* mice compared with *db/m*		Fold change of genes up- or downregulated in pioglitazone-treated *db/db* mice	
		5 weeks	7 weeks	Pioglitazone 3 mg/kg	Pioglitazone 15 mg/kg
Development related					
Upregulated					
Ephrin B2	U30244	2.11*	1.63*	1.63	1.20†
Glomerular epithelial protein 1 (PtrpO)	U37465	1.73*	1.16	2.70	1.55
Secreted frizzled related protein sFRP-2	U88567	1.69*	0.90	2.47	2.20
Cytoplasmic protein Ndrl	U60593	1.61*	2.23*	3.23	2.11
Transcriptional factor 21 (Podl)	AF035717	1.50*	0.61*	1.16†	0.93†
HIF-1α	Y09085	1.25	1.53*	1.83	1.13
Downregulated					
BTEB-1 (klf 9)	Y14296	0.46*	0.62*	0.70	1.01†
Iroquois homeobox protein 3	Y15001	0.61*	0.47*	0.34	1.64†
Cartilage-associated protein	AJ006469	0.62*	0.61*	0.80	1.35†
Glucose metabolism related					
Upregulated					
Phosphoglycerate mutase	AF029843	6.20*	5.47*	14.49	3.82
Transketolase	U05809	1.82*	1.91*	1.72	0.99†
Pyruvate kinase 3	X97047	1.78*	2.17*	2.23	1.32†
Glucose-6-phosphatase	U00445	1.61*	1.25	1.13	1.01
Phosphoenolpyruvate carboxykinase	AF009605	1.60*	1.64*	1.48	1.21
Pyruvate dehydrogenase kinase 3	AI853226	1.60*	2.12*	3.07	1.63
N-acetylneuraminate pyruvate lyase	AA710564	1.38	1.96*	3.15	1.08†
Downregulated					
Pyruvate dehydrogenase kinase 3	AI842259	0.48*	0.49*	0.47	1.26†
β-Galactosidase	M57734	0.57*	0.52*	0.63	1.16†
Vasoactive mediator related					
Upregulated					
Kallikrein	V00829	3.76*	4.26*	6.86	1.15†
Potential kallikrein gene	M13500	3.40*	3.86*	4.94	0.93
Epidermal growth factor–binding protein A	M1797	3.29*	3.96*	5.19	1.15†
Kallikrein 5	Y00500	3.24*	3.24*	3.66	0.81†
Mouse renin	M32352	2.93*	2.47*	3.31	1.43†
Glandular kallikrein	J00389	2.72*	2.65*	3.55	1.03†
Adrenomedullin	U77630	1.96*	2.52*	3.15	1.13
Serpin	M25529	1.69*	0.80	0.51	0.66
Carboxypeptidase N	AI182588	1.40*	2.11*	1.94	1.16†
Coagulation, fibrinolysis					
Upregulated					
Coagulation factor II receptor	AW123850	2.23*	1.91*	5.30	1.41
Protein S	L27439	1.61	1.86*	2.45	1.59
Tissue factor pathway inhibitor 2	D50586	1.38	2.17*	2.49	1.02†
Downregulated					
α2-ntiplasmin	Z36774	0.30*	0.34*	0.27	1.38†
Anticoagulant protein C	AF034569	0.46*	0.40*	0.46	0.84†
Cell structure					
Upregulated					
Tubulin β2	M28739	1.96*	2.79*	2.34	1.30
Calponin 3	AW125626	1.65*	1.57*	1.82	1.05
Tubulin α1	M28729	1.65*	1.32	1.78	1.13
(Podocyte structure)					
Dystroglycan 1	AV244370	1.38	1.69*	3.49	1.13†
Actinin 4 α	AI836968	1.22	1.60*	4.33	1.52
Apoptosis related					
Upregulated					
Clusterin	D14077	3.69*	4.37*	8.34	1.13†
Gelsolin	J04953	2.40*	1.69*	2.16	1.32
Downregulated					
Midkine	M34094	0.34*	0.56*	0.50	0.87
B-cell leukemia/lymphoma 6	U41465	0.44*	0.54*	1.11†	1.32†

Continued on following page

TABLE 2
Continued

Gene	ID	Fold change of genes up- or downregulated in *db/db* mice compared with *db/m*		Fold change of genes up- or downregulated in pioglitazone-treated *db/db* mice	
		5 weeks	7 weeks	Pioglitazone 3 mg/kg	Pioglitazone 15 mg/kg
Calcium-binding protein					
Upregulated					
Calbindin-28K	D26352	6.52*	9.97*	13.76	1.19†
Calcium-binding protein D-9k	AF028071	5.70*	7.21*	11.31	1.15†
Calcyclin	X66449	1.34	1.86*	3.29	1.24
Calcium-binding protein S100A1	AF087687	1.69*	1.57*	1.60	0.77
Steroid related					
Upregulated					
Hydroxysteroid 11-β-dehydrogenase 2	X90647	2.52*	3.86*	5.17	2.24
Glucocorticoid-regulated kinase	AW046181	2.12*	1.91*	3.07	1.28
Progesterone receptor membrane component 1	AF042491	1.34*	1.69*	2.51	0.98†
Downregulated					
Hydroxysteroid 17-β-dehydrogenase 11	AA822174	0.22*	0.20*	0.23	0.99†
Extracellular matrix component					
Upregulated					
Nephronectin	AA592182	1.82*	2.58*	4.69	1.91
Procollagen type IV (α1)	M15832	1.49	2.12*	3.58	1.65
Procollagen type XVIII (α1)	U03715	1.22	1.91*	1.72	1.72
Fibrosis related					
Upregulated					
Endoglin	X77952	2.34*	1.34	3.45	1.63
Connective tissue growth factor	M70642	1.87*	1.78*	4.05	1.87
Chaperone					
Downregulated					
Nucleoplasmin 3	U64450	0.45	0.46*	0.32	0.65
Cochaperone mt-GrpE#2	AF041060	0.80	0.54*	0.66	0.93†
Solute carrier family					
Upregulated					
Solute carrier family 8	AF004666	4.48*	7.89*	16.66	1.10†
Solute carrier family 3	AW122706	1.22	1.82*	2.71	1.40
Complement related					
Upregulated					
CD59 antigen	U60473	1.82*	1.61*	2.46	1.32
Downregulated					
C1q- and tumor necrosis factor–related protein 3	AI315647	0.48*	0.29*	0.42	1.30†
Others					
Upregulated					
WSB-1	AF033186	2.59*	6.69*	4.68	1.40†
Zinc finger protein 36	M58566	2.11*	1.35	2.28	1.55
Proline dehydrogenase 2	AA675075	1.96*	1.96*	1.90	0.69†
Smad 6	AF010133	2.11*	1.65	2.52	1.57
Cytotoxic T cell–associated protein 2	X15591	1.73*	0.89	1.93	1.20
Aldehyde dehydrogenase II	M74570	1.69*	2.11*	1.48	0.87†
Hephaestin	AF082567	1.68	2.86*	5.89	1.52†
α-Mannosidase II	X61172	1.49*	1.69*	2.23	1.03†
Carbonic anhydrase II	M25944	1.45*	1.92*	2.13	1.06†
Hexosaminidase A	U05837	1.38	1.69*	2.11	1.13
Protein tyrosine phosphatase receptor type D	D13903	1.25	1.87*	0.80	0.75†
Prominin-like 1	AF039663	1.13	2.12*	3.01	1.63
ROMK-2	AF012834	0.88	2.11*	1.11	1.03†
Downregulated					
CNDP dipeptidase 2	AI854839	0.08*	0.11*	0.08	0.85†
ATPase class VI 11a	AA690863	0.22*	0.22*	0.24	1.62†
UDP-glucuronosyltransferase 8	U48896	0.23*	0.21*	0.13	0.99†
Chemokine-like factor superfamily 6	AW125031	0.33*	0.34*	0.39	1.38†
Hepatic nuclear factor-1β	AB008174	0.42*	0.88	1.05	1.18

Continued on following page

TABLE 2
Continued

Gene	ID	Fold change of genes up- or downregulated in *db/db* mice compared with *db/m*: 5 weeks	Fold change of genes up- or downregulated in *db/db* mice compared with *db/m*: 7 weeks	Fold change of genes up- or downregulated in pioglitazone-treated *db/db* mice: Pioglitazone 3 mg/kg	Fold change of genes up- or downregulated in pioglitazone-treated *db/db* mice: Pioglitazone 15 mg/kg
Interferon regulatory protein 6	U73029	0.46*	0.88	1.07	1.18
Suppressor of cytokine signaling-2	U88327	0.46*	0.49	0.57	1.14
Uromodulin	L33406	0.47*	0.43*	0.72	1.29†
Carbonic anhydrase IV	U37091	0.49*	0.54*	0.45	1.14†
Connexin 26	M81445	0.49*	0.65	0.97	1.52†
Growth hormone receptor	U15012	0.52*	0.56*	0.48	0.97†
Aldehyde dehydrogenase 4	U14390	0.59*	0.53*	0.68	1.24†
Tripartite motif protein 47	AW048347	0.70	0.59*	0.54	1.02†
Carboxypeptidase H	X61232	0.45	0.17*	0.42†	1.78†
Makorin	AA656621	0.69	0.58*	0.45	0.95
Nitrilase 1	AF069988	0.74	0.59*	0.76	1.07†
Cyclophilin C	M74227	0.77	0.55*	0.64	0.95†

Gene names were ordered according to the absolute value of the relative log ratio. *Significant change compared with *db/m*, †significant change compared with untreated *db/db*, in comparison analysis by Microarray Suite 5.0.

(27), Pod-1 (28), glomerular epithelial protein 1 (GLEPP1) (29), and HIF-1α (30), in isolated glomeruli. These four genes are reported to play important roles in glomerulogenesis (27–30). Real-time RT-PCR confirmed significant mRNA elevation of ephrin B2 at 5 and 7 weeks of age (2.2- and 2.9-fold of control at 5 and 7 weeks of age, respectively) (Fig. 1*A*). Although the upregulation of HIF-1α was not significant by cDNA microarray analysis at 5 weeks of age, real-time RT-PCR revealed significant upregulation of HIF-1α mRNA at both 5 and 7 weeks of age (2.1- and 2.9-fold of control at 5 and 7 weeks of age, respectively) (Fig. 1*A*). Because HIF-1α is a transcription factor and it is more important to evaluate the expression of HIF-1α protein, we also examined HIF-1α protein expression by immunohistochemistry. HIF-1α protein expression was significantly increased in glomeruli at 7 weeks of age (Fig. 4*A*, *B*, and *D*). GLEPP1 and Pod-1 were significantly upregulated only at 5 weeks of age, and Pod-1 was significantly downregulated at 7 weeks (GLEPP1: 2.3- and 1.1-fold of control at 5 and 7 weeks of age; Pod-1: 4.0- and 0.5-fold, respectively) (Fig. 1*A*).

We also confirm the differential expression of podocyte

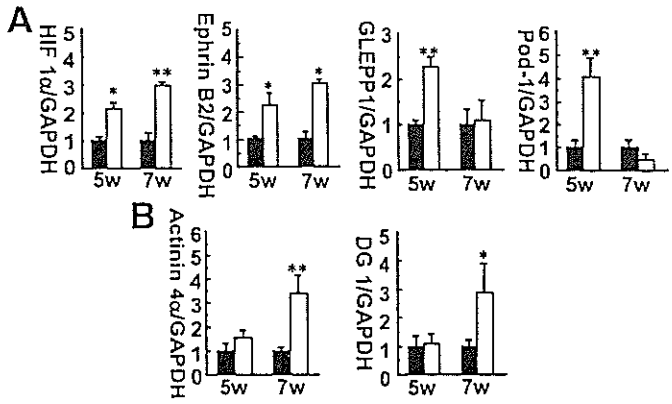

FIG. 1. mRNA expression of HIF-1α, ephrin B2, GLEPP1, and Pod-1 (*A*) and actinin 4α and DG1 (*B*) in isolated glomeruli from *db/m* and *db/db* mice at 5 and 7 weeks (w) of age by TaqMan real-time quantitative PCR. Values are the means ± SE, $n = 4$ for each group. *$P < 0.05$, **$P < 0.01$ vs. *db/m* mice. ■, *db/m* mice; □, *db/db* mice.

structure–related genes, actinin 4α (31) and dystroglycan 1 (DG1) (32), because morphologic changes of podocytes and podocyte injury play key roles in the development of diabetic nephropathy (3–6). Quantitative RT-PCR revealed significant upregulation of actinin 4α and DG1 in isolated glomeruli of 7- but not of 5-week-old *db/db* mice compared with those of control (actinin 4α: 3.4-fold; DG1: 2.9-fold) (Fig. 1*B*).

mRNA expression in cultured podocytes under high-glucose conditions. To examine whether the differential expression of kidney development–related genes and podocyte structure–related genes in isolated glomeruli of *db/db* mice could reflect the alteration in gene expression of podocytes, we next examined the expression of these genes in cultured podocytes by quantitative RT-PCR. Although Pod-1 mRNA expression was not detectable, ephrin B2, HIF-1α, GLEPP1, actinin 4α, and DG1 mRNA were detectable in cultured podocytes under normal glucose conditions. Ephrin B2 and HIF-1α mRNA expression was significantly upregulated under high-glucose conditions (5.7- and 2.3-fold of control, respectively) (Fig. 2*A*). GLEPP1 mRNA expression also tended to increase (1.6-fold of control) (Fig. 2*B*). By contrast, actinin 4α and DG1 mRNA did not show a significant change (Fig. 2*B*).

Comparison analysis of gene expression profile between *db/db* and pioglitazone-treated *db/db* mice. Insulin resistance is one of the important pathogenic factors for the diabetic nephropathy in type 2 diabetes. Indeed, improvement of insulin resistance by thiazolidinediones resulted in the reduction of albuminuria in diabetic nephropathy (33). Therefore, we examined the effects of pioglitazone on the gene expression profiles in *db/db* mice. Although administration of pioglitazone at a dose of 3 mg/kg did not affect hyperglycemia, insulin sensitivity, or albuminuria, pioglitazone at a dose of 15 mg/kg significantly reduced but did not normalize the blood glucose level, improved insulin sensitivity, and completely normalized urinary albumin excretion (Tables 3 and 4).

We first examined the effect of pioglitazone using microarray analysis. Table 2 shows genes in *db/db* mice whose differential expression was restored by pioglitazone

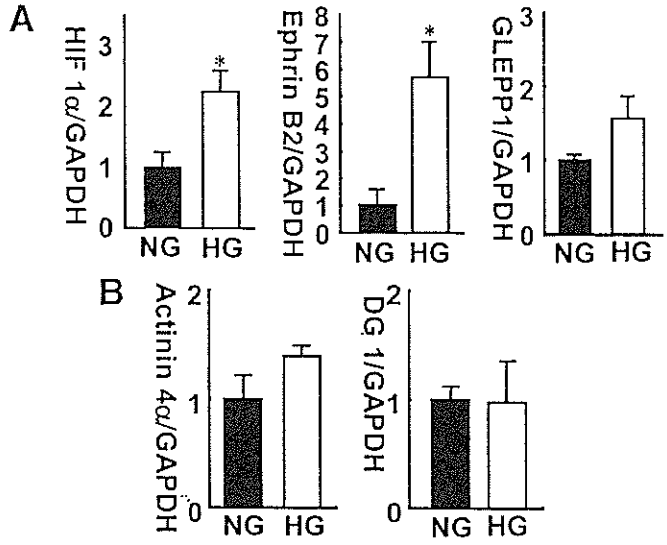

FIG. 2. mRNA expression of HIF-1α, ephrin B2, and GLEPP1 (*A*) and actinin 4α and DG1 (*B*) in cultured podocytes under high-glucose (HG) conditions by TaqMan real-time quantitative PCR. Values are the means ± SE. ■, normal glucose (NG; $n = 3$); □, high glucose ($n = 3$). *$P < 0.05$ vs. normal glucose. w, weeks.

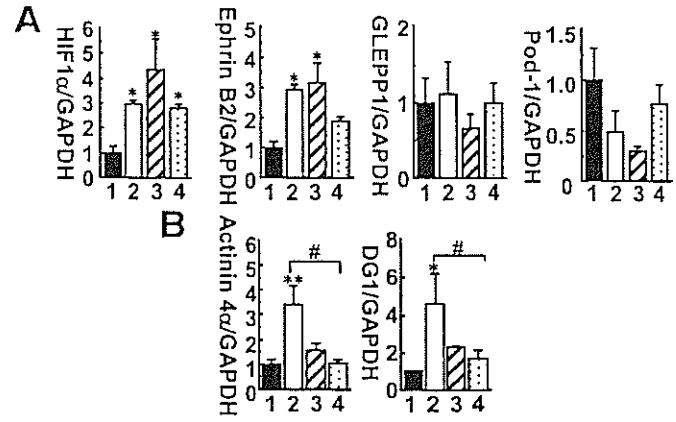

FIG. 3. mRNA expression of HIF-1α, ephrin B2, GLEPP1, and Pod-1 (*A*) and actinin 4α and DG1 (*B*) in isolated glomeruli from pioglitazone-treated *db/db* mice by TaqMan real-time quantitative PCR. 1, *db/m* mice; 2, untreated *db/db* mice; 3, *db/db* mice treated with 3 mg/kg pioglitazone; 4, *db/db* mice treated with 15 mg/kg pioglitazone. Values are the means ± SE, $n = 4$ for each group. *$P < 0.05$, **$P < 0.01$ vs. *db/m* mice; #$P < 0.05$.

treatment. Although the lower dose of pioglitazone (3 mg/kg) restored only a small number of genes (4 of 116), pioglitazone at the higher dose restored the alteration in more than two-thirds of the genes (81 of 116) in *db/db* mice. Pioglitazone restored most of the genes related to oxidative stress (16 of 17), lipid metabolism (11 of 14), glucose metabolism (4 of 8), development (5 of 7), cell growth (6 of 9), vasoactive mediator (6 of 8), and coagulation (3 of 5). Among these genes, the recovery of oxidative stress–, glucose metabolism–, and lipid metabolism–related gene expression by pioglitazone was compatible with previous reports (34,35). By contrast, only a small number of the genes related to fibrosis (0 of 2), apoptosis (1 of 3), calcium-binding protein (2 of 4), cell structure (1 of 5), and extracellular matrix component (0 of 3) were restored by pioglitazone.

We also examined mRNA expression of kidney development– and podocyte structure–related genes by quantitative RT-PCR. Upregulation of ephrin B2 and downregulation of Pod-1 were blunted by pioglitazone treatment (Fig. 3*A*). Although suppression of HIF-1α mRNA expression was not observed in microarray analysis and RT-PCR, HIF-1α protein expression was partially attenuated by pioglitazone (Fig. 4). Upregulation of actinin 4α and DG1 genes was significantly attenuated by pioglitazone treatment (Fig. 3*B*).

DISCUSSION

Although glomerular injury plays a central role in the development of diabetic nephropathy, most reports using microarray analysis have focused on the gene expression profile of the whole kidney in diabetic animals with nephropathy. In the current study, we examined a gene expression profile of isolated glomeruli from *db/db* mice, a well-known type 2 diabetes model. To the best of our knowledge, this is the first report on the glomerular gene expression profile in type 2 diabetes models. Our microarray data showed differential expression of genes related to glucose and lipid metabolism, oxidative stress, vasoactive mediators, cell growth, and coagulation in isolated glomeruli between *db/db* and *db/m* mice at the normoalbuminuric stage. These results are compatible with previous reports (1–3).

Our first new finding is that the kidney development–related genes were already differentially expressed at the normoalbuminuric stage in the glomeruli of *db/db* mice. Although the pathophysiological significance of the kidney development–related genes we examined is not fully clarified in diabetic nephropathy, ephrin B2, HIF 1α, Pod-1, and GLEPP1 participate in various stages and aspects of glomerulogenesis and are relevant to some types of glomerular injury, as previously suggested (26). Ephrin B2 is a transmembrane ligand of the ephrin B2 receptor (Eph) and its signaling pathway is required for vascular morphogenesis (36,37) and glomerular microvascular assembly (27). HIF-1α is critical for renal vasculogenesis and glomerulogenesis (30), and nuclear localization of HIF-1α increases in murine adriamycin nephrosis (38). Nyengaad and Rasch (39) reported an increase in glomerular capillary size and number in diabetic nephropathy, suggesting that angiogenesis is associated with glomerular injury. Actually, vascular endothelial growth factor (VEGF) plays a key role in the development of proteinuria and glomerular sclerosis in diabetic nephropathy (14). Although VEGF mRNA were not elevated at the normoalbuminuric

TABLE 3
Blood glucose levels of insulin tolerance test in *db/db* mice

	0 min	20 min	60 min	100 min	160 min
Untreated *db/db*	157 ± 56	135 ± 75	63 ± 12	91 ± 10	120 ± 13
db/db + 3 mg/kg pioglitazone	148 ± 30	172 ± 13	67 ± 9	94 ± 4	131 ± 4
db/db + 15 mg/kg pioglitazone	117 ± 9	87 ± 6	58 ± 7	38 ± 78*	53 ± 15*

Data are the means ± SE. Each group has $n = 4$. *$P < 0.01$ vs. untreated *db/db*.